ordpy: A Python package for data analysis with permutation entropy and ordinal network methods

Arthur A. B. Pessa[1, a)] and Haroldo V. Ribeiro[1, b)]

Departamento de Física, Universidade Estadual de Maringá – Maringá, PR 87020-900,
Brazil

Since Bandt and Pompe's seminal work, permutation entropy has been used in several applications and is now an essential tool for time series analysis. Beyond becoming a popular and successful technique, permutation entropy inspired a framework for mapping time series into symbolic sequences that triggered the development of many other tools, including an approach for creating networks from time series known as ordinal networks. Despite the increasing popularity, the computational development of these methods is fragmented, and there were still no efforts focusing on creating a unified software package. Here we present ordpy, a simple and open-source Python module that implements permutation entropy and several of the principal methods related to Bandt and Pompe's framework to analyze time series and two-dimensional data. In particular, ordpy implements permutation entropy, Tsallis and Rényi permutation entropies, complexity-entropy plane, complexity-entropy curves, missing ordinal patterns, ordinal networks, and missing ordinal transitions for one-dimensional (time series) and two-dimensional (images) data as well as their multiscale generalizations. We review some theoretical aspects of these tools and illustrate the use of ordpy by replicating several literature results.

Permutation entropy is a complexity measure and data analysis tool stemming from nonlinear time series analysis and information theory. In the almost two decades since its conception, this method has gained prominence and become extensively studied and used by researchers from several fields. The concept of ordinal patterns introduced with permutation entropy has also inspired a whole ecosystem of related techniques, including an approach to map time series into networks known as ordinal networks. However, this ecosystem of tools still lacks a more comprehensive numerical implementation, limiting the further spreading of ordinal methods, especially to fields with less tradition in developing computational tools. In this article, we present ordpy – an open-source Python package implementing several tools related to ordinal patterns for the analysis of time series and images. We present ordpy's functionalities together with a review of all pertinent theoretical developments, replicate several literature results, and highlight possible developments of ordinal methods that can be explored with ordpy.

I. INTRODUCTION

Stemming from a combination of ideas from nonlinear time series analysis[1,2] and information theory[3], permutation entropy was first introduced in 2002 by Bandt and Pompe[4] as a simple, robust, and computationally efficient complexity measure for time series. This complexity measure is defined as the Shannon entropy of a probability distribution associated with ordinal patterns evaluated from partitions of a time series – a procedure known as the Bandt-Pompe symbolization approach. Permutation entropy and its underlying symbolization approach have become increasingly popular among researchers working with time series analysis, leading to successful applications in fields as diverse as biomedical sciences[5], econophysics[6], physical sciences[7], and engineering[8]. The uses of permutation entropy also span a large variety of goals such as monitoring the dynamical regime of a system[8], detecting anomalies in time series[7], characterizing time series data[5], testing for serial independence[9], and are further documented in review articles by Zanin *et al.*[10], Riedl *et al.*[11], Amigó *et al.*[12], and Keller *et al.*[13].

Permutation entropy's success is not limited to its practical usage as this approach has inspired numerous time series analysis tools. Some of these related methods consider different quantifiers for the ordinal probability distribution[14–24], generalize the Bandt-Pompe symbolization algorithm to evaluate ordinal structures on multiple temporal scales[25–28], include signal amplitude information[29–32], and account for equal values in time series[33,34]. Other works have generalized permutation entropy and its ordinal approach to two-dimensional data such as images[35,36]. The ordinal patterns underlying permutation entropy have also been used for mapping time series and images into networks known as ordinal networks[37–43].

The original version of permutation entropy and its various generalizations represent an essential and appealing framework for data analysis, especially when considering the increasing availability of large data sets[44]

---

a)Electronic mail: arthur_pessa@hotmail.com
b)Electronic mail: hvr@dfi.uem.br

and the steady demand for reliable and computationally efficient methods for extracting meaningful information from these data sets[45,46]. However, most methods emerging from Bandt and Pompe's seminal work lack freely available computational implementation, and the exceptions are limited to a single or very few approaches. Here we help to fill this gap by presenting `ordpy` – a simple and open-source Python module implementing several of the principal methods related to Bandt and Pompe's framework. This module has been designed to be easily set up and installed as its only dependency is `numpy`[47], a fundamental Python library implementing array objects and fast math functions that operate on these objects. Beyond our preferences, the Python programming language has been chosen for its widespread use in scientific computing[47] and extensive community support[48].

We present `ordpy`'s functions and illustrate their usage along with a review of the pertinent theoretical developments of permutation entropy and its related ordinal methods. Our work alternates between the mathematical description of the different techniques and the presentation of functions and code snippets that implement these data analysis tools. We further use `ordpy` to replicate several literature results. The source-code of `ordpy` is freely available on its git repository (github. com/arthurpessa/ordpy) together with the documentation of all `ordpy`'s functions (arthurpessa.github.io/ ordpy). We can install `ordpy` using the Python Package Index (PyPI) via:

```
$ pip install ordpy
```

We further provide the code and data for replicating all analyses presented in this article as a Jupyter notebook[49,50] on `ordpy`'s website.

II. AN OVERVIEW OF ORDINAL DISTRIBUTIONS, PERMUTATION ENTROPY, AND COMPLEXITY-ENTROPY PLANE

We start by presenting a short review of Bandt and Pompe's seminal permutation entropy[4]. As we have already mentioned, permutation entropy is the Shannon entropy of a probability distribution related to ordinal (or permutation) patterns evaluated using sliding partitions over a time series. This probability distribution is the so-called ordinal distribution or distribution of ordinal patterns, and the symbolization process used to estimate this distribution is the Bandt-Pompe approach. To describe this process, let us consider an arbitrary time series $\{x_t\}_{t=1,\ldots,N_x}$. First, we divide this time series into $n_x = N_x - (d_x - 1)\tau_x$ overlapping partitions comprised of $d_x > 1$ observations separated by $\tau_x \geq 1$ time units. For given values of d_x and τ_x, each data partition can be represented by

$$w_p = (x_p, x_{p+\tau_x}, x_{p+2\tau_x}, \ldots, x_{p+(d_x-2)\tau_x}, x_{p+(d_x-1)\tau_x}), \ (1)$$

where $p = 1, \ldots, n_x$ is the partition index. The parameters d_x and τ_x are the only two parameters of the Bandt-Pompe method: d_x is the embedding dimension[4] and τ_x is the embedding delay[26]. It is worth remarking that Bandt and Pompe's original proposal was restricted to $\tau_x = 1$ (that is, data partitions comprised of consecutive time series elements), and the embedding delay was further introduced by Cao *et al.*[51] and Zunino *et al.*[26]. As we shall see, the choices of d_x and τ_x are important, and there is research exclusively devoted to determining optimal values for these parameters[11,52,53].

Next, for each partition w_p, we evaluate the permutation $\pi_p = (r_0, r_1, \ldots, r_{d_x-1})$ of the index numbers $(0, 1, \ldots, d_x - 1)$ that sorts the elements of w_p in ascending order, that is, the permutation of the index numbers defined by the inequality $x_{p+r_0} \leq x_{p+r_1} \leq \cdots \leq x_{p+r_{d_x-1}}$. In case of equal values, we maintain the occurrence order of the partition elements, that is, if $x_{p+r_{k-1}} = x_{p+r_k}$ then $r_{k-1} < r_k$ for $k = 1, \ldots, d_x - 1$[51]. As an illustration, suppose we have $x_t = (5, 3, 2, 2, 7, 9)$ and set $d_x = 4$ and $\tau_x = 1$. The first partition is $w_1 = (5, 3, 2, 2)$, and sorting its elements we find $2 \leq 2 < 3 < 5$ or $x_{1+2} \leq x_{1+3} < x_{1+1} < x_{1+0}$. Thus, the permutation symbol (ordinal pattern) associated with w_1 is $\pi_1 = (2, 3, 1, 0)$. Another possibility for dealing with ties among partition elements consists in adding a small noise perturbation without modifying all other ordering relations. This latter scheme was initially proposed in Bandt and Pompe's seminal work, but it is much less used in the literature. In most cases, time series data have enough resolution for making these equalities negligible; however, this issue can become critical for low-resolution signals[54].

After evaluating the permutation symbols associated with all data partitions, we obtain a symbolic sequence $\{\pi_p\}_{p=1,\ldots,n_x}$. The `ordpy`'s function `ordinal_sequence` returns this sequence as illustrated in the following code:

```
>>> from ordpy import ordinal_sequence
>>> x = [5, 3, 2, 2, 7, 9]
>>> ordinal_sequence(x, dx=4, taux=1)
array([[2, 3, 1, 0],
       [1, 2, 0, 3],
       [0, 1, 2, 3]])
>>> ordinal_sequence([1.55, 1.54, 1.53], dx=2)
array([[1, 0], [1, 0]])
>>> ordinal_sequence([1.55, 1.54, 1.53], dx=2,
... tie_precision=1)
array([[1, 0], [0, 1]])
```

The last two examples illustrate the use of parameter `tie_precision` that defines the number of decimals considered for establishing the ordinal relations. This parameter is available in most `ordpy`'s functions and is particularly relevant when working with time series presenting equal values that could be mistaken by floating-point number representation. Figure 1(a) illustrates the application of the Bandt-Pompe approach for a simple time series and different values of d_x and τ_x.
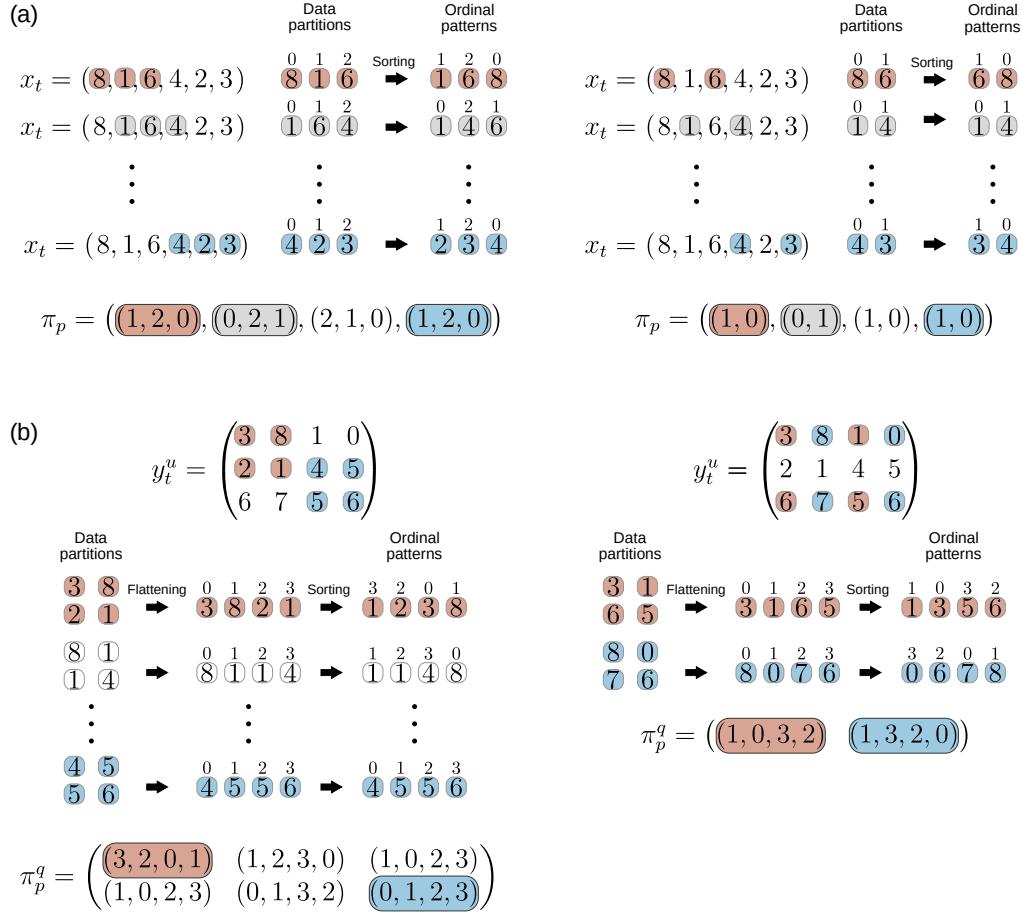
The ordinal probability distribution $P \quad =$

(a)

Data partitions → Ordinal patterns

$$x_t = (8, 1, 6, 4, 2, 3) \quad \overset{0\ 1\ 2}{8\ 1\ 6} \xrightarrow{\text{Sorting}} \overset{1\ 2\ 0}{1\ 6\ 8}$$

$$x_t = (8, 1, 6, 4, 2, 3) \quad \overset{0\ 1\ 2}{1\ 6\ 4} \rightarrow \overset{0\ 2\ 1}{1\ 4\ 6}$$

$$\vdots$$

$$x_t = (8, 1, 6, 4, 2, 3) \quad \overset{0\ 1\ 2}{4\ 2\ 3} \rightarrow \overset{1\ 2\ 0}{2\ 3\ 4}$$

$$\pi_p = \big((1,2,0), (0,2,1), (2,1,0), (1,2,0) \big)$$

Data partitions → Ordinal patterns

$$x_t = (8, 1, 6, 4, 2, 3) \quad \overset{0\ 1}{8\ 6} \xrightarrow{\text{Sorting}} \overset{1\ 0}{6\ 8}$$

$$x_t = (8, 1, 6, 4, 2, 3) \quad \overset{0\ 1}{1\ 4} \rightarrow \overset{0\ 1}{1\ 4}$$

$$\vdots$$

$$x_t = (8, 1, 6, 4, 2, 3) \quad \overset{0\ 1}{4\ 3} \rightarrow \overset{1\ 0}{3\ 4}$$

$$\pi_p = \big((1,0), (0,1), (1,0), (1,0) \big)$$

(b)

$$y_t^u = \begin{pmatrix} 3 & 8 & 1 & 0 \\ 2 & 1 & 4 & 5 \\ 6 & 7 & 5 & 6 \end{pmatrix}$$

Data partitions → Ordinal patterns

$$\begin{matrix} 3 & 8 \\ 2 & 1 \end{matrix} \xrightarrow{\text{Flattening}} \overset{0\ 1\ 2\ 3}{3\ 8\ 2\ 1} \xrightarrow{\text{Sorting}} \overset{3\ 2\ 0\ 1}{1\ 2\ 3\ 8}$$

$$\begin{matrix} 8 & 1 \\ 1 & 4 \end{matrix} \rightarrow \overset{0\ 1\ 2\ 3}{8\ 1\ 1\ 4} \rightarrow \overset{1\ 2\ 3\ 0}{1\ 1\ 4\ 8}$$

$$\vdots$$

$$\begin{matrix} 4 & 5 \\ 5 & 6 \end{matrix} \rightarrow \overset{0\ 1\ 2\ 3}{4\ 5\ 5\ 6} \rightarrow \overset{0\ 1\ 2\ 3}{4\ 5\ 5\ 6}$$

$$\pi_p^q = \begin{pmatrix} (3,2,0,1) & (1,2,3,0) & (1,0,2,3) \\ (1,0,2,3) & (0,1,3,2) & (0,1,2,3) \end{pmatrix}$$

$$y_t^u = \begin{pmatrix} 3 & 8 & 1 & 0 \\ 2 & 1 & 4 & 5 \\ 6 & 7 & 5 & 6 \end{pmatrix}$$

Data partitions → Ordinal patterns

$$\begin{matrix} 3 & 1 \\ 6 & 5 \end{matrix} \xrightarrow{\text{Flattening}} \overset{0\ 1\ 2\ 3}{3\ 1\ 6\ 5} \xrightarrow{\text{Sorting}} \overset{1\ 0\ 3\ 2}{1\ 3\ 5\ 6}$$

$$\begin{matrix} 8 & 0 \\ 7 & 6 \end{matrix} \rightarrow \overset{0\ 1\ 2\ 3}{8\ 0\ 7\ 6} \rightarrow \overset{3\ 2\ 0\ 1}{0\ 6\ 7\ 8}$$

$$\pi_p^q = \big((1,0,3,2) \quad (1,3,2,0) \big)$$

FIG. 1. The symbolization process of Bandt and Pompe. (a) Illustration of Bandt-Pompe method applied to a time series and the resulting ordinal sequences for embedding parameters $d_x = 3$ and $\tau_x = 1$ (left) and $d_x = 2$ and $\tau_x = 2$ (right). (b) Application of the two-dimensional version of the Bandt-Pompe method to a data array and the resulting ordinal sequences for embedding parameters $d_x = d_y = 2$ and $\tau_x = \tau_1 = 1$ (left) and $d_x = d_y = 2$ and $\tau_x = \tau_1 = 2$ (right). In both panels, the colored boxes indicate the data partitioning scheme for each set of embedding parameters, and the numbers above them represent the index numbers used for determining the ordinal patterns or permutation symbols.

$\{\rho_i(\Pi_i)\}_{i=1,\dots,n_\pi}$ is simply the relative frequency of all possible permutations within the symbolic sequence, that is,

$$\rho_i(\Pi_i) = \frac{\text{number of partitions of type } \Pi_i \text{ in } \{\pi_p\}}{n_x}, \quad (2)$$

where Π_i represents each one of the $n_\pi = d_x!$ different ordinal patterns. The following code shows how to obtain the ordinal distribution with `ordpy`'s function `ordinal_distribution`:

```
>>> from ordpy import ordinal_distribution
>>> x = [5, 3, 2, 2, 7, 9]
>>> pis, rho = ordinal_distribution(x, dx=3)
>>> pis
array([[0, 1, 2],
       [1, 2, 0],
       [2, 1, 0]])
>>> rho
array([0.5 , 0.25, 0.25])
```

The two arrays returned by `ordinal_distribution` are the ordinal patterns and their corresponding relative frequencies, respectively. By default, `ordinal_distribution` does not return non-occurring permutations (that is, those with $\rho_i(\Pi_i) = 0$); however, the parameter `return_missing` modifies this behavior as in:

```
>>> from ordpy import ordinal_distribution
>>> x = [5, 3, 2, 2, 7, 9]
>>> pis, rho = ordinal_distribution(x, dx=3,
... return_missing=True)
>>> pis
array([[0, 1, 2],
       [1, 2, 0],
       [2, 1, 0],
       [0, 2, 1],
       [1, 0, 2],
       [2, 0, 1]])
>>> rho
```

```
array([0.5 , 0.25, 0.25, 0.  , 0.  , 0.  ])
```

Missing permutation symbols are always the latest elements of the returned array.

Having the ordinal probability distribution P, we can calculate its Shannon entropy[3] and define the permutation entropy as

$$S(P) = -\sum_{i=1}^{n_\pi} \rho_i(\Pi_i) \log \rho_i(\Pi_i), \quad (3)$$

where $\log(\dots)$ stands for the base-2 logarithm. Permutation entropy quantifies the randomness in the ordering dynamics of a time series such that $S \approx \log n_\pi$ indicates a random behavior, while $S \approx 0$ implies a more regular dynamics. Because the maximum value of S is $S_{\max} = \log n_\pi$, we can further define the normalized permutation entropy as

$$H(P) = \frac{S(P)}{\log n_\pi}, \quad (4)$$

where the values of H are restricted to the interval $[0,1]$. The `ordpy`'s function `permutation_entropy` calculates the values of S and H directly from a time series as illustrated in:

```
>>> from ordpy import permutation_entropy
>>> x = [5, 3, 2, 2, 7, 9]
>>> permutation_entropy(x)
0.5802792108518123
>>> permutation_entropy(x, normalized=False,
... base='e')
1.0397207708399179
```

The `permutation_entropy` function uses the base-2 logarithm function by default; however, the parameter `base` can modify this behavior.

The embedding dimension d_x defines the number of possible permutations ($n_\pi = d_x!$), and following Bandt and Pompe's recommendation[4], it is common to choose the values of $d_x \in \{3,4,5,6,7\}$ to satisfy the condition $d_x! \ll N_x$ to obtain a reliable estimate of the ordinal probability distribution. Another less common choice is to use a value of d_x such that $5d_x! \le N_x$[55]. More recently, however, Cuesta-Frau *et al.*[52] have shown that these requirements on d_x can be considerably loosened in several situations related to classification tasks. The embedding delay τ_x defines a time scale for the system under analysis and is often set as 1; however, different values of τ_x may inform about delayed feedback mechanisms and time-correlation structures. We present a more detailed discussion about the choices of d_x and τ_x in Appendix A.

The permutation entropy framework was extended to two-dimensional data by Ribeiro *et al.*[35] and Zunino and Ribeiro[36]. To present this generalization, let us consider an arbitrary two-dimensional data array $\{y_t^u\}_{t=1,\dots,N_x}^{u=1,\dots,N_y}$ whose elements may represent pixels of an image. We further define the embedding dimensions d_x and d_y along the horizontal and vertical directions (respectively), and

the corresponding embedding delays τ_x and τ_y. Similarly to the one-dimensional case, we slice the data array in partitions of size $d_x \times d_y$ defined by

$$w_p^q = \begin{pmatrix} y_p^q & y_{p+\tau_x}^q & \cdots & y_{p+(d_x-1)\tau_x}^q \\ y_p^{q+\tau_y} & y_{p+\tau_x}^{q+\tau_y} & \cdots & y_{p+(d_x-1)\tau_x}^{q+\tau_y} \\ \vdots & \vdots & \ddots & \vdots \\ y_p^{q+(d_x-1)\tau_x} & y_{p+\tau_x}^{q+(d_x-1)\tau_x} & \cdots & y_{p+(d_x-1)\tau_x}^{q+(d_y-1)\tau_y} \end{pmatrix}, \quad (5)$$

where the indexes $p = 1,\dots,n_x$ and $q = 1,\dots,n_y$, with $n_x = N_x - (d_x-1)\tau_x$ and $n_y = N_y - (d_y-1)\tau_y$, cover all $n_x n_y$ data partitions. To associate a permutation symbol with each two-dimensional partition, we flatten the partitions w_p^q line by line, that is,

$$\begin{aligned} w_p^q = \big(&y_p^q, y_{p+\tau_x}^q, \dots, y_{p+(d_x-1)\tau_x}^q, \\ &y_p^{q+\tau_y}, y_{p+\tau_x}^{q+\tau_y}, \dots, y_{p+(d_x-1)\tau_x}^{q+\tau_y}, \dots, \\ &y_p^{q+(d_x-1)\tau_x}, y_{p+\tau_x}^{q+(d_x-1)\tau_x}, \dots, y_{p+(d_x-1)\tau_x}^{q+(d_y-1)\tau_y}\big). \end{aligned} \quad (6)$$

As this procedure does not depend on a particular partition, we can simplify the notation by representing w_p^q as

$$w_p^q = \big(\tilde{y}_0, \tilde{y}_1, \dots, \tilde{y}_{d_x d_y - 2}, \tilde{y}_{d_x d_y - 1}\big), \quad (7)$$

where $\tilde{y}_0 = y_p^q$, $\tilde{y}_1 = y_{p+\tau_x}^q$, and so on. Then, we evaluate the permutation symbol associated with each data partition as in the one-dimensional case to define the symbolic array $\{\pi_p^q\}_{p=1,\dots,n_x}^{q=1,\dots,n_y}$ related to the data set (Fig. 1b illustrates the Bandt-Pompe approach for two-dimensional data). From this array, we calculate the relative frequency for all $n_\pi = (d_x d_y)!$ possible permutations Π_i via

$$\rho_i(\Pi_i) = \frac{\text{number of partitions of type } \Pi_i \text{ in } \{\pi_p^q\}}{n_x n_y}, \quad (8)$$

where $i = 1,\dots,n_\pi$, and so the ordinal probability distribution is $P = \{\rho_i(\Pi_i)\}_{i=1,\dots,n_\pi}$. It is worth noticing that the ordering procedure defining the permutation symbols is no longer unique as in the one-dimensional case. For instance, we would find a different symbolic array by flattening the partitions w_p^q column by column. However, different ordering procedures do not modify the set of elements comprising the ordinal probability distribution (only their order is changed)[35].

As in the one-dimensional case, the two-dimensional permutation entropy is simply the Shannon entropy of the ordinal distribution $P = \{\rho_i(\Pi_i)\}_{i=1,\dots,n_\pi}$, so we can calculate the two-dimensional permutation entropy and its normalized version using Eqs. 3 and 4, respectively. Only the total number of possible ordinal patterns ($n_\pi = (d_x d_y)!$ in the two-dimensional case) is modified.

Similarly to the one-dimensional case, the values of d_x and d_y are usually constrained by the condition $(d_x d_y)! \ll N_x N_y$ in order to obtain a reliable estimate

of the ordinal distribution P[35,36]. Naturally, this two-dimensional formulation recovers the one-dimensional case ($N_y = 1$ for time series data) by setting $d_y = \tau_y = 1$. In `ordpy`, the functions `ordinal_sequence`, `ordinal_distribution` and `permutation_entropy` automatically implement this two-dimensional generalization when the input data is a two-dimensional array as in:

```
>>> from ordpy import ordinal_sequence,
... ordinal_distribution, permutation_entropy
>>> y = [[5, 3, 2], [2, 7, 9]]
>>> ordinal_sequence(y, dx=2, dy=2)
array([[[2, 1, 0, 3],
        [1, 0, 2, 3]]])
>>> ordinal_distribution(y, dx=2, dy=2)
(array([[1, 0, 2, 3],
        [2, 1, 0, 3]]), array([0.5, 0.5]))
>>> permutation_entropy(y, dx=2, dy=2)
0.21810429198553155
```

In addition to permutation entropy, the complexity-entropy plane proposed by Rosso et al.[14] is another popular time series analysis tool directly related to Bandt and Pompe's symbolization approach. This method was initially introduced for distinguishing between chaotic and stochastic time series but has been successfully used as an effective discriminating tool in several other contexts[56–60]. The complexity-entropy plane combines the normalized permutation entropy H (Eq. 4) with an intensive statistical complexity measure C (also calculated using the ordinal distribution) to build a two-dimensional representation space with the values of C versus H. The statistical complexity C used by Rosso et al. is inspired by the work of Lopez-Ruiz et al.[61] and is defined by the product of the normalized permutation and a normalized version of the Jensen-Shannon divergence[62] between the ordinal distribution $P = \{\rho_i(\Pi_i)\}_{i=1,\dots,n_\pi}$ and the uniform distribution $U = \{1/n_\pi\}_{i=1,\dots,n_\pi}$ (it is worth remembering that n_π is the number of possible ordinal patterns). Mathematically, we can write this measure as

$$C(P) = \frac{D(P,U)H(P)}{D^{\max}}, \qquad (9)$$

where

$$D(P,U) = S[(P+U)/2] - \frac{1}{2}S(P) - \frac{1}{2}S(U) \qquad (10)$$

is the Jensen-Shannon divergence and

$$D^{\max} = -\frac{1}{2}\left(\frac{n_\pi!+1}{n_\pi!}\log(n_\pi!+1) - 2\log(2n_\pi!) + \log n_\pi!\right)$$

is a normalization constant. This latter constant expresses the maximum possible value of $D(P,U)$ occurring for $P = \{\delta_{1,i}\}_{i=1,\dots,n_\pi}$[63,64], where $\delta_{ij} = \begin{cases} 1 & \text{if } i = j \\ 0 & \text{if } i \neq j \end{cases}$ is the Kronecker delta function.

Differently from permutation entropy, the statistical complexity C is zero in both extremes of order (when only one permutation symbol occurs) and disorder (when all permutations are equally likely to happen). The value of C quantifies structural complexity and provides additional information that is not carried by the value of H. Furthermore, C is a nontrivial function of H in the sense that for a given value of H, there exists a range of possible values for C[14,63,64]. This happens because H and D are expressed by different sums of $\rho_i(\Pi_i)$ and there is thus no reason for assuming a univocal relationship between H and C.

To better illustrate this feature, let us assume (for simplicity) we replace the Jensen-Shannon divergence by the Euclidean distance between P and U (as in the seminal work of Lopez-Ruiz et al.[61]), that is, $D(P,U) = \sum_{i=1}^{n_\pi}(\rho_i(\Pi_i) - 1/n_\pi)^2$. In this case, the statistical complexity is

$$C(P) \propto -\left(\sum_{i=1}^{n_\pi}\rho_i(\Pi_i)\log\rho_i(\Pi_i)\right)\left(\sum_{i=1}^{n_\pi}(\rho_i(\Pi_i)-1/n_\pi)^2\right),$$

and we can readily observe that different ordinal distributions $P = \{\rho_i(\Pi_i)\}_{i=1,\dots,n_\pi}$ may lead to the same value of H but different values of C (or vice-versa). Let us further consider a particular ordinal distribution with three possible permutation symbols (this would be equivalent to having $d_x! = 3$ or $(d_x d_y)! = 3$, if possible), that is, $P = \{a, b, 1 - (a+b)\}$, where $a > 0$ and $b > 0$ are real numbers such that $(a+b) \leq 1$ (to ensure the normalization of P). For this case, we have $S = -a\log a - b\log b - [1 - (a+b)]\log[1 - (a+b)]$ and $D = (a-1/3)^2 + (b-1/3)^2 + ([1-(a+b)]-1/3)^2$. Thus, for instance, if $a = 0.79$ and $b = 0.18$ or $a = 0.80$ and $b = 0.16$ we find the same value of $H = S/\log 3 \approx 0.55$, but different values for D (0.32 in the first case and 0.33 in the second) and, consequently, for C.

In `ordpy`, the `complexity_entropy` function simultaneously returns the values of H and C from time series as illustrated in:

```
>>> from ordpy import complexity_entropy
>>> complexity_entropy([4,7,9,10,6,11,3],
... dx=2)
(0.918295834054894, 0.06112816548804511)
```

Furthermore, the complexity-entropy plane was generalized for two-dimensional data[35,36] (notice that the only changes are related to the process of estimating the ordinal distribution) and the `complexity_entropy` function also accepts two-dimensional arrays as input as shown in:

```
>>> from ordpy import complexity_entropy
>>> complexity_entropy([[1,2,1],[8,3,4],
... [6,7,5]], dx=2, dy=2)
(0.3271564379782973, 0.2701200547320647)
```
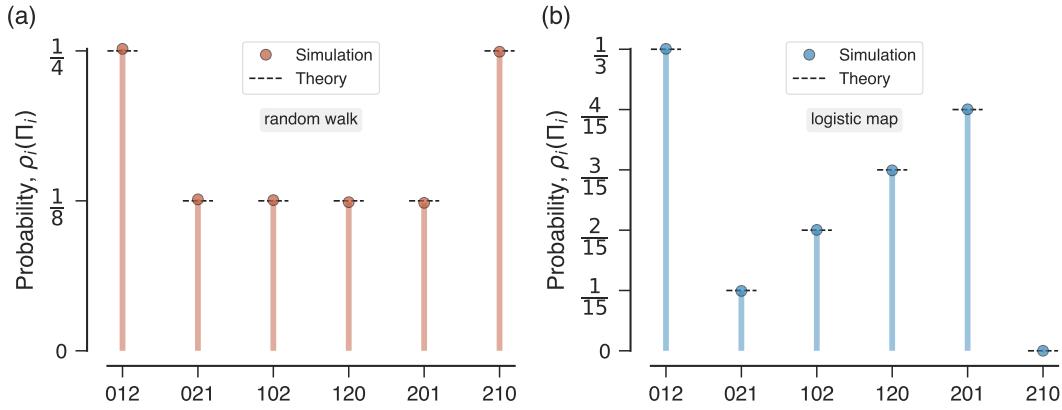
FIG. 2. Probability distributions of ordinal patterns for stochastic and deterministic series. (a) Comparison between the empirical probability distribution of ordinal patterns obtained from a simulated Gaussian random walk with 10^6 steps and the exact distribution P_{walk} (dashed horizontal lines) for $d_x = 3$ and $\tau_x = 1$. (b) Comparison between the empirical probability distribution of ordinal patterns obtained from 10^6 iterations of the logistic map at fully developed chaos and the exact distribution P_{logistic} (dashed horizontal lines) for $d_x = 3$ and $\tau_x = 1$. All results in this figure can be replicated by running a Jupyter notebook available at ordpy's webpage.

III. APPLICATIONS OF BANDT AND POMPE'S FRAMEWORK WITH ORDPY

This section presents more engaging applications of ordpy's functions by replicating literature results. We start by determining the ordinal probability distributions of two different time series of stochastic and chaotic nature, namely, a random walk with Gaussian steps and the logistic map at fully developed chaos (see Appendix B for definitions). We choose these two examples because their ordinal distributions are exactly known for some combinations of the embedding parameters[65,66]. More specifically, for $d_x = 3$ and $\tau_x = 1$, the probability distributions associated with the permutation symbols $\{(0,1,2),(0,2,1),(1,0,2),(1,2,0),(2,0,1),(2,1,0)\}$ are $P_{\text{walk}} = \{1/4, 1/8, 1/8, 1/8, 1/8, 1/4\}$ and $P_{\text{logistic}} = \{1/3, 1/15, 2/15, 3/15, 4/15, 0\}$ for the random walk[66] and the logistic map[65], respectively.

To numerically estimate these two ordinal distributions, we generate a time series from a Gaussian random walk process and another time series from iterations of the fully chaotic logistic map. In both cases, we have simulated one realization of each process with 10^6 observations and used the ordinal_distribution function. Figure 2 shows that the exact ordinal distributions are in excellent agreement with simulated results obtained with ordpy. It is intriguing to observe that the ordinal pattern $(2,1,0)$ ("descending permutation") does not occur in the logistic series (it has probability zero). This fact is best understood as a feature directly associated with the intrinsic determinism of the logistic map dynamics[65,67]. As we shall discuss in the next section, investigations about such "missing ordinal patterns" are also useful for characterizing time series dynamics.

To better illustrate the use of the permutation_entropy function, we partially repro-

duce Bandt and Pompe's analysis of the logistic map (Fig. 2 of Ref. 4). We generate time series consisting of 10^6 iterations of the logistic map for each value of parameter $r \in \{3.5, 3.5001, 3.5002, \ldots, 4.0\}$ (see Appendix B for definitions). Next, we calculate the permutation entropy S for each of these 5001 time series using permutation_entropy with embedding parameters $d_x = 6$ and $\tau_x = 1$. We further divide the permutation entropy by 5 to obtain the permutation entropy per symbol of order 6, that is, $h_6 = S/5$ as defined in Bandt and Pompe's work[4]. Figure 3a depicts the well-known bifurcation diagram for the logistic map, while Fig. 3b shows the values of h_6 as a function of the parameter r. We note that the permutation entropy per symbol has an overall increasing trend with the parameter r, marked by abrupt drops in intervals of r related to periodic behaviors. As noticed by Bandt and Pompe, the behavior of the permutation entropy is similar to the one observed for the Lyapunov exponent[4].

In another example with permutation_entropy, we replicate a numerical experiment of Cao et al.[51] (see their Fig. 1) that searches for dynamical changes in the transient logistic map time series (see Appendix B for definitions). This problem illustrates the role of the embedding delay τ_x. As in the original article, we iterate the transient logistic map starting with the initial condition $x_0 = 0.65$ and incrementing the logistic parameter r from 2.8 to 4 in steps of size 10^{-5}. This process generates a time series with 120001 observations as shown in Fig. 3c. Using this time series, we calculate the normalized permutation entropy within a sliding window with 1024 observations for the embedding dimension $d_x = 5$ and two values for the embedding delay ($\tau_x = 1$ and $\tau_x = 2$).

As Cao et al.[51], we denote the permutation entropy values by $H[r(t)]$, where $r(t)$ represents the logistic parameter at the end of the sliding window. Figure 3d
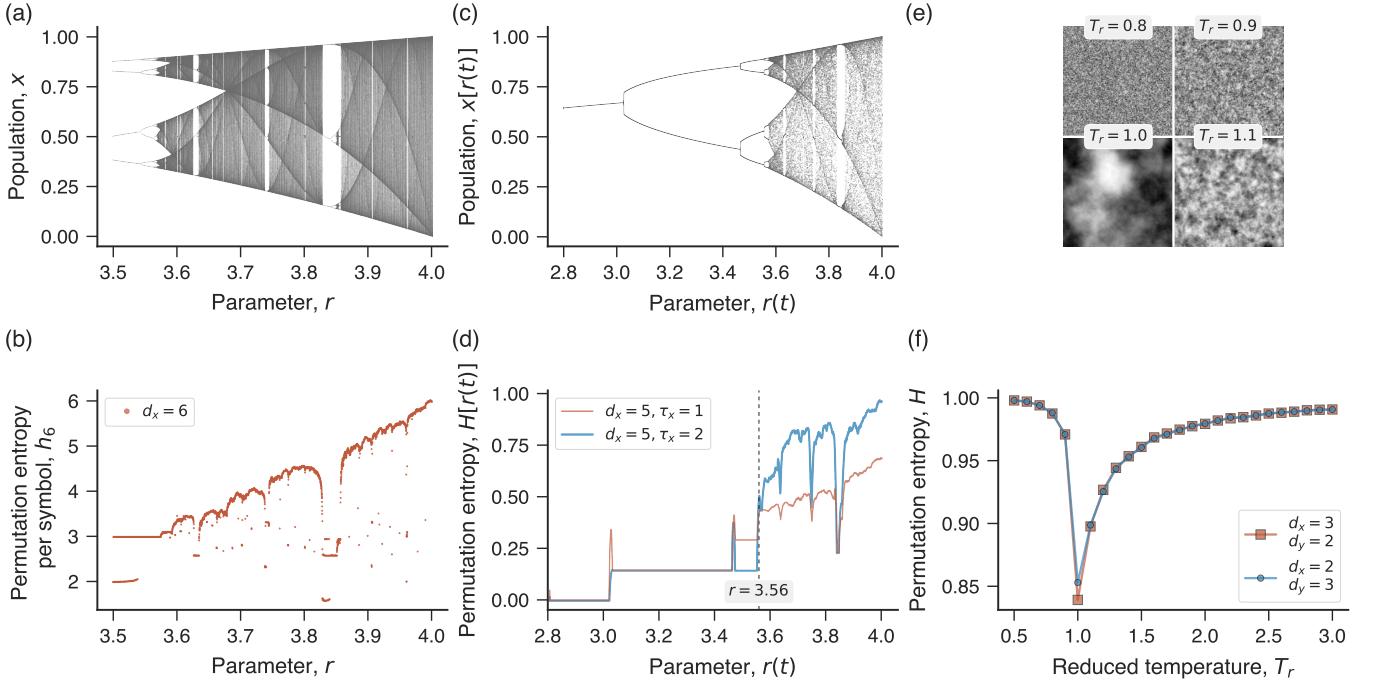
FIG. 3. Permutation entropy of one- and two-dimensional data. (a) Bifurcation diagram of the logistic map for r between 3.5 and 4 in steps of size 10^{-4}. (b) Permutation entropy per symbol of order six (h_6) calculated from logistic time series with 10^6 observations (random initial conditions) and $r \in \{3.5, 3.5001, 3.5002, \ldots, 4.0\}$. The embedding parameters are $d_x = 6$ and $\tau_x = 1$. (c) Time series of the transient logistic map obtained from the initial condition $x_0 = 0.65$, and by incrementing the logistic parameter r at each iteration from 2.8 to 4 in steps of size 10^{-5}. Despite appearing very similar to a bifurcation diagram, this result refers to a time series where each observation $x[r(t)]$ corresponds to a value $r(t)$. (d) Dependence of the normalized permutation entropy evaluated within a sliding window with 1024 observations of the original time series. Here $r(t)$ represents the logistic parameter at the end of each sliding window. The different curves show the results for $d_x = 5$ and $\tau_x = 1$ (red), and $d_x = 5$ and $\tau_x = 2$ (blue). The vertical line at $r = 3.56$ indicates the period-8 to period-16 bifurcation. (e) Ising surfaces obtained after 10^6 Monte Carlo steps with reduced temperatures $T_r \in \{0.8, 0.9, 1.0, 1.1\}$. In these surfaces, dark gray shades indicate high lattice sites while light gray regions indicate the opposite. (f) Normalized permutation entropy as a function of the reduced temperature $T_r \in \{0.5, 0.6, \ldots, 3.0\}$ for Ising surfaces of size 250×250 obtained after 10^6 Monte Carlo steps. The different curves show the results for embedding parameters $d_x = 3$ and $d_y = 2$ (red) and $d_x = 2$ and $d_y = 3$ (blue), both with $\tau_x = \tau_y = 1$. All results in this figure can be reproduced by running a Jupyter notebook available at ordpy's webpage.

shows the values of $H[r(t)]$, where abrupt changes are clearly associated with dynamical changes observed in the time series (Fig. 3c). Despite the overall similarities, we note that the embedding delay $\tau_x = 2$ identifies these dynamical changes better than the case with $\tau_x = 1$; for instance, the transition from period-8 to period-16 (at $r \approx 3.56$) is missed when $\tau_x = 1$ but captured when $\tau_x = 2$[51].

As we have mentioned, a generalization of permutation entropy to two-dimensional data was first proposed by Ribeiro *et al.*[35]. To illustrate the use of the permutation_entropy function with two-dimensional data, we replicate a numerical experiment related to Ising surfaces (see Appendix C for definitions) present in that work (Fig. 8 of Ref. 35). These surfaces represent the accumulated sum of spin variables of the canonical two-dimensional Ising model in a Monte Carlo simulation. Figure 3e shows four examples of these surfaces (square lattices of size 250×250) obtained after 10^6 Monte Carlo steps for different reduced temperatures T_r. We notice

non-trivial patterns emerging when the reduced temperature is equal to the critical temperature ($T_r = 1$) of phase transition for the Ising model[68]. Following the original article, we generate Ising surfaces (size 250×250) for reduced temperatures $T_r \in \{0.5, 0.6, \ldots, 3.0\}$ and calculate their normalized permutation entropy with $d_x = 3$ and $d_y = 2$, and $d_x = 2$ and $d_y = 3$, both for $\tau_x = \tau_y = 1$. In agreement with Ribeiro *et al.*[35], Fig. 3f shows that the permutation entropy precisely identifies the phase transition of the Ising model (the sudden decrease around the critical temperature) and that these Ising surfaces are symmetric under reversal of the embedding dimensions.

The complexity_entropy function simultaneously calculates the permutation entropy and the statistical complexity from time series and image data. To illustrate its usage, we partially reproduce the results of Rosso *et al.*[14] (Fig. 1 in that work) on distinguishing chaotic from stochastic time series. By following their article, we iterate four discrete maps to generate chaotic series. Specifically, we obtain chaotic time series from skew tent
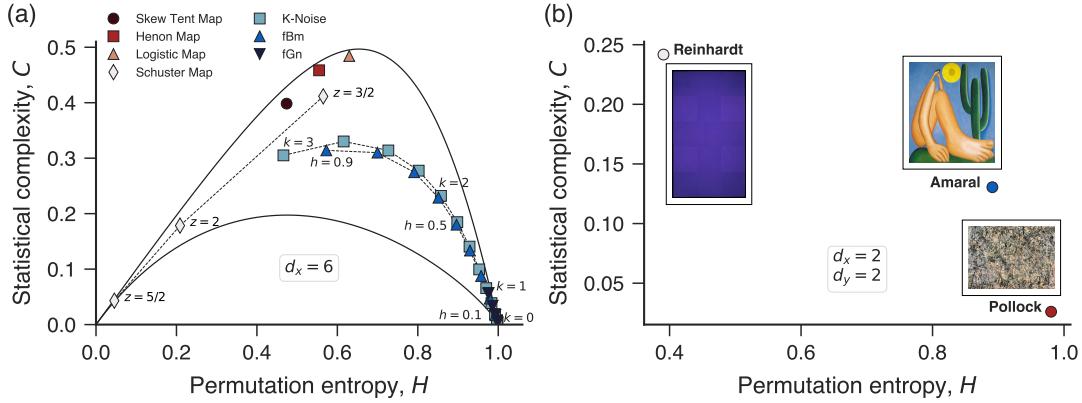
FIG. 4. Complexity-entropy plane for one- and two-dimensional data. (a) Average values of the statistical complexity C versus the normalized permutation entropy H (over ten realizations) evaluated from time series of chaotic maps and stochastic processes. The embedding parameters are $d_x = 6$ and $\tau_x = 1$. The solid lines represent the maximum and minimal possible values of complexity for a given entropy (for $d_x = 6$ and $\tau_x = 1$). (b) Localization of three art paintings in the complexity-entropy plane with embedding parameters $d_x = d_y = 2$ and $\tau_x = \tau_y = 1$. All data and code necessary to reproduce this figure are available in a Jupyter notebook at `ordpy`'s webpage.

map (parameter $w = 0.1847$), Hénon map (x-component, parameters $a = 1.4$ and $b = 0.3$), logistic map ($r = 4$), and Schuster map (parameter $z \in \{3/2, 2, 5/2\}$) – see Appendix B for definitions. We further generate stochastic series from three stochastic processes: noises with $1/f^{-k}$ power spectrum (for $k \in \{0.00, 0.25, \dots, 3.00\}$), fractional Brownian motion (Hurst exponent $h \in \{0.1, 0.2, \dots, 0.9\}$), and fractional Gaussian noise (also $h \in \{0.1, 0.2, \dots, 0.9\}$) – see Appendix C for definitions. For each of these maps and stochastic processes, we generate ten time series with 2^{15} observations and random initial conditions. Next, we use `complexity_entropy` with embedding parameters $d_x = 6$ and $\tau_x = 1$ to calculate their statistical complexity and permutation entropy (average values over 10 time series realizations).

As in the original work of Rosso *et al.*[14], Fig. 4a shows that chaotic series usually have high complexity and low entropy values. Stochastic time series, in turn, display high entropy and intermediary complexity values. It is also interesting to note that stochastic time series approach the lower-right corner of the complexity-entropy plane ($H \to 1$ and $C \to 0$) as the serial auto-correlation decreases[14]. These results also illustrate that some stochastic and chaotic series have very similar entropy values but different statistical complexity (for instance, fractional Brownian motion with $h = 0.9$ and Schuster map with $z = 3/2$), confirming that the statistical complexity extracts additional information from the ordinal distribution. In this figure, we have also included two solid lines delimiting the accessible region of the complexity-entropy plane[64]. In `ordpy`, the functions `maximum_complexity_entropy` and `minimum_complexity_entropy` generate these curves, as shown in the following code snippet:

```
>>> from ordpy import
... maximum_complexity_entropy,
```

```
... minimum_complexity_entropy
>>> maximum_complexity_entropy(dx=4)
array([[-0.        , -0.        ],
       [ 0.21810429,  0.19670592],
       [ 0.34568712,  0.28362016],
       ...
       [ 0.98660828,  0.02388382]])
>>> minimum_complexity_entropy(dx=4)
array([[-0.00000000e+00, -0.00000000e+00],
       [ 2.67076969e-02,  2.55212327e-02],
       ...
       [ 1.00000000e+00, -3.66606083e-16]])
```

The `complexity_entropy` function also works with two-dimensional data, and to illustrate its usage, we follow Sigaki *et al.*[69] and use the complexity-entropy plane to investigate patterns in art paintings. Due to the large-scale of the data analyzed by Sigaki *et al.* and to keep our examples self-contained, we do not reproduce their original results but simply use their ideas to illustrate how complexity and entropy extract useful information from images. To do so, we handpick three paintings from wikiart.org (in the original article, the authors studied 137,364 images obtained from the same webpage). These are a Color Field Painting artwork (Blue, 1953 by Ad Reinhardt, image size 768×435[70]), a Brazilian Modernist artwork (Abaporu, 1928 by Tarsila do Amaral, image size 1200×1026[71]), and an American Abstract Expressionist painting (Number 1, 1950 (Lavender Mist), 1950 by Jackson Pollock, image size 749×1024[72]). The three images are in JPEG format with 24 bits per pixel (8 bits for red, green, and blue colors in the RGB color space). We have averaged the pixels over the three RGB layers to represent each image by a usual two-dimensional array. Having these arrays, we calculate the statistical complexity and permutation entropy for the three paintings with embedding parameters $d_x = d_y = 2$ and $\tau_x = \tau_y = 1$.

Figure 4b shows the complexity-entropy plane for these images (insets depict the artworks). In agreement with the global trend observed by Sigaki *et al.*[69], these results show that paintings portraying objects with clearly defined borders (such as the squares in Reinhardt's artwork) tend to present large values of statistical complexity and low values of entropy. On the other extreme, paintings with smudged and diffuse contours (such as Pollock's drip paintings) have high entropy and low complexity values. Between these somewhat opposite behaviors, we have a whole continuum of images, as exemplified here by the work of the Brazilian painter Tarsila do Amaral. As argued by Sigaki *et al.*[69], the complexity-entropy plane maps the local degree of order of artworks into a scale of order-disorder and simplicity-complexity that is similar to qualitative descriptions of artworks proposed by art historians such as Wölfflin (the linear versus painterly dichotomy) and Riegl (the haptic versus optic dichotomy).

IV. MISSING ORDINAL PATTERNS

As we have commented, the logistic map at fully developed chaos does not exhibit the "descending permutation" $(2,1,0)$ for $d = 3$ (see Fig. 2b). This feature is not a particularity of the logistic map. Indeed, these missing ordinal patterns (also called forbidden patterns) occur in different systems, and simple statistics associated with them have proven to be useful and reliable indicators of a system's dynamics[6,73–76]. The works of Amigó *et al.*[65,67] are seminal in this regard, and by following their classification, we can divide these forbidden ordinal patterns into two categories: true or false[67]. True forbidden patterns (such as the $(2,1,0)$ in the logistic map) are a fingerprint of determinism in a time series dynamics and represent an intrinsic feature of the underlying dynamical process[65]; that is, these patterns are not an artifact related to the finite length of empirical observations. In turn, false forbidden patterns are related to the finite length of time series[67] and can emerge even from completely random processes.

This distinction is not straightforward when dealing with empirical data, but a typical analysis in this context consists in investigating the number of missing patterns (η) as a function of the time series length (N_x). The behavior of this curve is useful for discriminating time series. In `ordpy`, the `missing_patterns` function identifies missing ordinal patterns and estimates their relative frequency as in:

```
>>> from ordpy import missing_patterns
>>> missing_patterns([4,7,9,10,6,11,3,5,
... 6,2,3,1], dx=3)
(array([[0, 2, 1],
        [2, 1, 0]]),
 0.333333333333333)
```

To better illustrate the use of this function, we inves-

tigate missing ordinal patterns in time series obtained from the logistic map at fully developed chaos ($r = 4$) and Gaussian random walks. In both cases, we use the embedding dimensions $d_x = 5$ and $d_x = 6$ (with $\tau_x = 1$) and series lengths $N_x \in \{60, 150, 240, \ldots, 6000\}$. Figure 5a shows the results. We observe that the number of missing ordinal patterns approaches zero as the time series length of random walks increases. Conversely, the number of missing permutations related to the logistic map displays an initial decay with the time series length but it rapidly saturates in considerably large numbers, indicating that these missing patterns are intrinsically associated with the underlying determinism of the process[67].

In another application with the `missing_patterns` function, we replicate a result of Amigó *et al.*[67] (Fig. 4 in their work) to further show that the number of missing patterns is a good indicator of determinism in time series[55,67]. By following the original work, we generate time series from the logistic map at fully developed chaos (6000 iterations) and add to them uniformly distributed noise in the interval $[-\xi, \xi]$, where ξ is the noise amplitude. Next, we estimate the average number of missing patterns (over ten time series replicas) for each noise level $\xi \in \{0, 0.001, 0.002, \ldots, 0.5\}$, and embedding dimensions $d_x = 5$ and $d_x = 6$ (with $\tau_x = 1$). Figure 5b shows the number of missing ordinal patterns as a function of noise amplitude ξ for both embedding dimensions. We observe that the number of missing patterns related to these deterministic series contaminated with noise approaches zero as noise amplitude grows. However, significantly higher noise levels are necessary to remove all signs of determinism expressed by the lack of permutation patterns when $d_x = 6$[67].

V. TSALLIS AND RÉNYI ENTROPY-BASED QUANTIFIERS OF THE ORDINAL DISTRIBUTION

In addition to Shannon's entropy and the statistical complexity, researchers have proposed to use other quantifiers of the ordinal probability distribution[15,19,22,39]. As we have explicitly verified for the statistical complexity, these different quantifiers are supposed to extract additional information from a time series' dynamics that is not captured by permutation entropy and statistical complexity. In this context, a productive approach is to consider parametric generalizations of Shannon's entropy, such as those proposed by Tsallis[77] and Rényi[78]. The work of Zunino *et al.*[15] was the first to consider the Tsallis entropy in place of Shannon's entropy to define the Tsallis permutation entropy as

$$S_\beta(P) = \frac{1}{\beta - 1} \sum_{i=1}^{n_\pi} \left(\rho_i(\Pi_i) - \rho_i(\Pi_i)^\beta \right), \quad (11)$$

where β is a real parameter ($\beta \to 1$ recovers the usual Shannon entropy and so the permutation entropy). Tsallis's entropy is also maximized by the uniform distribution, such that $S_\beta^{\max} = \frac{1 - (n_\pi)^{1-\beta}}{\beta - 1}$. Thus, the normalized
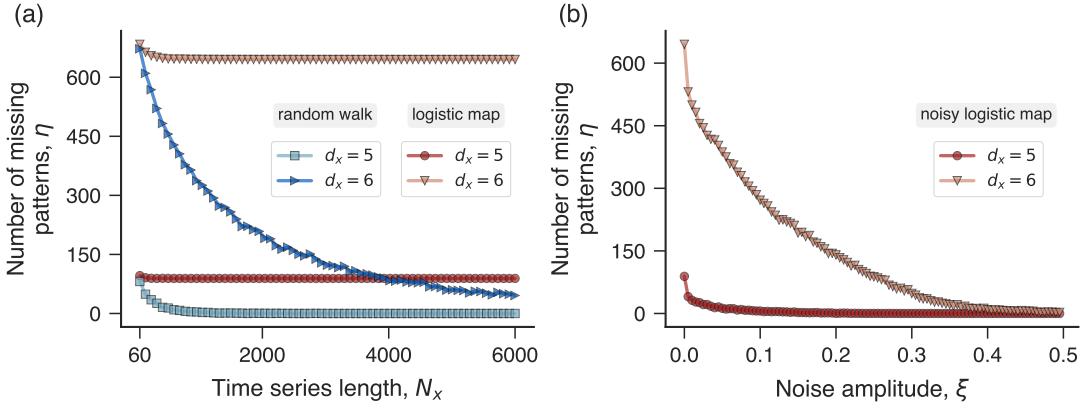
FIG. 5. Missing ordinal patterns in time series. (a) Number of missing ordinal patterns (η) in random walk (blue) and logistic map (red) time series as a function of sequence length (N_x) for embedding parameters $d_x = 5$ and $d_x = 6$, both with $\tau_x = 1$. Results represent the average number of missing permutations over ten time series replicas for each $N_x \in \{60, 150, 240, \ldots, 6000\}$. (b) Dependence of the number of missing ordinal patterns on the noise intensity (ξ) for noisy logistic time series with 6000 observations. The noise added to the logistic series is uniformly distributed in the interval $[-\xi, \xi]$ with $\xi \in \{0, 0.001, 0.002, \ldots, 0.5\}$. Results represent average values over ten time series replicas for each noise level. The embedding dimensions are indicated within the plot and the embedding delay is $\tau_x = 1$. We use random initial conditions and set the parameter $r = 4$ in all experiments with the logistic map. The necessary code to reproduce these results is available in a Jupyter notebook at ordpy's webpage.

Tsallis permutation entropy is

$$H_\beta(P) = (\beta - 1)\frac{S_\beta(P)}{1 - (n_\pi)^{1-\beta}}. \tag{12}$$

Similarly, Liang et al.[19] have proposed the Rényi permutation entropy

$$S_\alpha(P) = \frac{1}{1-\alpha}\ln\left(\sum_{i=1}^{n_\pi}\rho_i(\Pi_i)^\alpha\right), \tag{13}$$

where $\alpha > 0$ is a real parameter. Rényi's entropy converges to Shannon's entropy when $\alpha \to 1$ and is maximized by the uniform distribution ($S_\alpha^{\max} = \ln n_\pi$, as the usual Shannon entropy). Thus, the normalized Rényi permutation entropy is

$$H_\alpha(P) = \frac{S_\alpha(P)}{\ln n_\pi}. \tag{14}$$

In both cases, the generalized entropic form is monoparametric and has a term where the ordinal probabilities appear raised to the power of the entropic parameter (that is, $\rho_i(\Pi_i)^\beta$ and $\rho_i(\Pi_i)^\alpha$). These parameters assign different weights to the underlying ordinal probabilities, allowing us to access different dynamical scales and produce a family of quantifiers for the ordinal distribution. In ordpy, the tsallis_entropy and renyi_entropy functions implement these two quantifiers as in:

```
>>> from ordpy import tsallis_entropy,
... renyi_entropy
>>> tsallis_entropy([4,7,9,10,6,11,3],
... q=[1,2], dx=2) #Here q plays the
```

```
... role of beta.
array([0.91829583, 0.88888889])
>>> renyi_entropy([4,7,9,10,6,11,3],
... alpha=[1,2], dx=2)
array([0.91829583, 0.84799691])
```

In a similar direction, there are also the developments of complexity-entropy curves proposed by Ribeiro et al.[23] and Jauregui et al.[24]. These works have further extended the complexity-entropy plane concept by considering the Tsallis and Rényi entropies combined with proper generalizations of statistical complexity[64]. Thus, instead of having a single point in the complexity-entropy plane for a given time series, Ribeiro et al.[23] and Jauregui et al.[24] have created parametric curves by varying the entropic parameter (β or α) and simultaneously calculating the generalized entropy and the generalized statistical complexity.

To define the Tsallis complexity-entropy curves[23], we first extend the statistical complexity (Eq. 9) using the Tsallis entropy, that is,

$$C_\beta(P) = \frac{D_\beta(P,U)H_\beta(P)}{D_\beta^{\max}}, \tag{15}$$

where

$$D_\beta(P,U) = \frac{1}{2}K_\beta\left(P\left|\frac{P+U}{2}\right.\right) + \frac{1}{2}K_\beta\left(U\left|\frac{P+U}{2}\right.\right) \tag{16}$$

is the Jensen-Tsallis divergence[64] written in terms of the corresponding Kullback-Leibler divergence[64,79]

$$K_\beta(V|R) = \frac{1}{\beta-1}\sum_i^{n_\pi} v_i^\beta\left[r_i^{1-\beta} - v_i^{1-\beta}\right], \tag{17}$$

where $V = \{v_i\}_{i=1,\ldots,n_\pi}$ and $R = \{r_i\}_{i=1,\ldots,n_\pi}$ are two arbitrary distributions. In Eq. 15,

$$D_\beta^{\max} = \frac{2^{2-\beta} n_\pi - (1+n_\pi)^{1-\beta} - n_\pi(1+1/n_\pi)^{1-\beta} - n_\pi + 1}{2^{2-\beta} n_\pi (1-\beta)}$$

is a normalization constant representing the maximum possible value of $D_\beta(P,U)$ that occurs for $P = \{\delta_{1,i}\}_{i=1,\ldots,n_\pi}$ (as in the usual Jensen-Shannon divergence). By following Ribeiro *et al.*[23], we construct a parametric representation of the ordered pairs $(H_\beta(P), C_\beta(P))$ for $\beta > 0$, obtaining the Tsallis complexity-entropy curves.

Similarly, to define the Rényi complexity-entropy curves[24], we generalize the statistical complexity in Rényi's formalism as

$$C_\alpha(P,U) = \frac{D_\alpha(P,U)H_\alpha(P)}{D_\alpha^{\max}}, \qquad (18)$$

where

$$D_\alpha(P,U) = \frac{1}{2}K_\alpha\left(P\left|\frac{P+U}{2}\right.\right) + \frac{1}{2}K_\alpha\left(U\left|\frac{P+U}{2}\right.\right) \quad (19)$$

is the Jensen-Rényi divergence[64] written in terms of

$$K_\alpha(V|R) = \frac{1}{\alpha-1}\ln\left(\sum_{i=1}^{d!} v_i^\alpha r_i^{1-\alpha}\right), \qquad (20)$$

the corresponding Kullback-Leibler divergence for Rényi's entropy[64,80]. The normalization constant

$$D_\alpha^{\max} = \frac{1}{2(\alpha-1)}\ln\left[\frac{(n_\pi+1)^{1-\alpha} + n_\pi - 1}{n_\pi}\left(\frac{n_\pi+1}{4n_\pi}\right)^{1-\alpha}\right]$$

corresponds to the maximum possible value of $D_\alpha(P,U)$ occurring for $P = \{\delta_{1,i}\}_{i=1,\ldots,n_\pi}$ (as in the usual Jensen-Shannon divergence). Again, we can construct a parametric representation of the ordered pairs $(H_\alpha(P), C_\alpha(P))$ for $\alpha > 0$, obtaining the Rényi complexity-entropy curves proposed by Jauregui *et al.*[24].

In ordpy, the functions tsallis_complexity_entropy and renyi_complexity_entropy implement the Tsallis and Rényi complexity-entropy curves as shown in the following code snippet:

```
>>> from ordpy import
... tsallis_complexity_entropy,
... renyi_complexity_entropy
>>> tsallis_complexity_entropy(
... [4,7,9,10,6,11,3],
... dx=2, q=[1,2]) #Here q plays the
... role of beta.
array([[0.91829583, 0.06112817],
       [0.88888889, 0.07619048]])
>>> renyi_complexity_entropy(
... [4,7,9,10,6,11,3],
... dx=2, alpha=[1, 2])
array([[0.91829583, 0.06112817],
       [0.84799691, 0.08303895]])
```

To better illustrate the use of these ordpy's functions, we replicate some numerical experiments involving the logistic map and random walks presented in the original works of Ribeiro *et al.*[23] (Figs. 1 and 6 in that work) and Jauregui *et al.*[24] (Figs. 1 and 3 in that work). We start by generating time series from the logistic map at fully developed chaos ($r = 4$, random initial condition) and a Gaussian random walk. For the logistic map series, we discard the first 10^4 iterations to avoid transient effects and iterate other 10^6 steps. The random walk series also has 10^6 observations. By using these time series, we generate their corresponding Tsallis complexity-entropy curves for $d_x = 3$ and $\tau_x = 1$ by sampling 10^3 log-spaced values of the entropic parameter β between 0.01 and 100 for the logistic map, and between 0.001 and 100 for the random walk.

Figures 6a and 6b show the empirical complexity-entropy curves in comparison with their exact shape (dashed lines). These theoretical curves can be determined for these time series because the ordinal distributions of the logistic map ($P_{\text{logistic}} = \{1/3, 1/15, 2/15, 3/15, 4/15, 0\}$) and random walks ($P_{\text{walk}} = \{1/4, 1/8, 1/8, 1/8, 1/8, 1/4\}$) are exactly known for $d_x = 3$[65,66]. We observe that theoretical and empirical results are in excellent agreement. As discussed by Ribeiro *et al.*[23], random series tend to form closed complexity-entropy curves (Fig. 6b), while chaotic time series are usually represented by open complexity-entropy curves (Fig. 6a). These features emerge as a direct consequence of the existence or not of missing ordinal patterns captured by the limiting behavior of H_β as $\beta \to 0$ and $\beta \to \infty$[23].

By following a similar approach, we also estimate the Rényi complexity-entropy curves for the two previous time series for $d_x = 4$ and $\tau_x = 1$. Figures 6c and 6d show these Rényi complexity-entropy curves. Differently from the Tsallis case, Rényi complexity-entropy curves are always open[24], and the usage of these curves for distinguishing chaotic from stochastic series relies on a more subtle characteristic. Indeed, Jauregui *et al.*[24] have found that the initial curvature of Rényi complexity-entropy curves (dC_α/dH_α for small α) can be used as an indicative of determinism in time series. Specifically, they found that positive curvatures are associated with time series of stochastic nature, while negative ones are related to chaotic phenomena. This pattern also occurs in the results of Figs. 6c and 6d.

VI. ORDINAL NETWORKS

Among the more recent developments related to the Bandt-Pompe framework, we have the so-called ordinal networks. First proposed by Small[37] for investigating nonlinear dynamical systems, and later generalized with his collaboration in a series of works[38,81–83], ordinal networks belong to a more general class of methods designed to map time series into networks, collectively
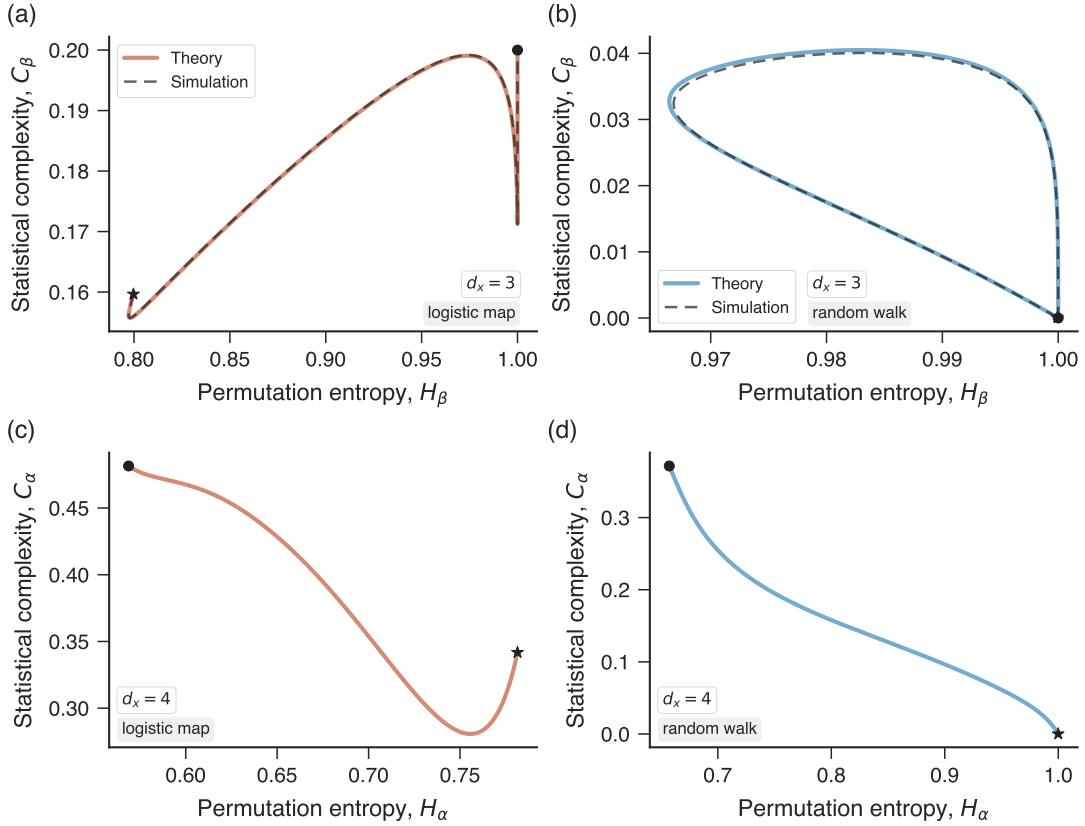
FIG. 6. Tsallis and Rényi complexity-entropy curves. Tsallis complexity-entropy curves for time series obtained from (a) the logistic map at fully developed chaos and (b) a Gaussian random walk, both with embedding parameters $d_x = 3$ and $\tau_x = 1$. The solid lines represent the empirical results and the dashed lines indicate the exact form of these complexity-entropy curves. Panels (c) and (d) show the Rényi complexity-entropy curves obtained from the same two time series with embedding parameters $d_x = 4$ and $\tau_x = 1$. In all panels, star markers indicate the beginning of the curves ($\beta \approx 0$ or $\alpha \approx 0$), while circle markers indicate the end of the curves (largest values of β and α). Data and code necessary to reproduce these results are available in a Jupyter notebook at `ordpy`'s webpage.

known as time series networks[84]. Beyond counting ordinal patterns, this approach considers first-order transitions among ordinal symbols within a symbolic sequence. In this network representation, the different ordinal patterns occurring in a data set are mapped into nodes of a complex network. The edges between nodes indicate that the associated permutation symbols are adjacent to each other in a symbolic sequence. Furthermore, edges can be directed according to the temporal succession of ordinal symbols and weighted by the relative frequencies in which the corresponding successions occur in a symbolic sequence[38].

After applying the Bandt-Pompe method with embedding parameters d_x and τ_x to a time series $\{x_t\}_{t=1,\ldots,N_x}$ and obtaining the symbolic sequence $\{\pi_p\}_{p=1,\ldots,n_x}$, we can define the elements of the weighted adjacency matrix of the corresponding ordinal network as[38,40]

$$\rho_{i,j} = \frac{\text{total of transitions } \Pi_i \to \Pi_j \text{ in } \{\pi_p\}_{p=1,\ldots,n_x}}{n_x - 1},$$

(21)

where $i, j = 1, 2, \ldots, n_\pi$ (with $n_\pi = d_x!$), Π_i and Π_j rep-

resent all possible ordinal patterns, and the denominator $n_x - 1$ is the total number of ordinal transitions. In `ordpy`, the `ordinal_network` function returns the nodes, edges, and edge weights of an ordinal network mapped from a time series as in:

```
>>> from ordpy import ordinal_network
>>> ordinal_network([4,7,9,10,6,11,8,3,7],
... dx=2, normalized=False)
(array(['0|1', '1|0'], dtype='<U3'),
 array([['0|1', '0|1'],
        ['0|1', '1|0'],
        ['1|0', '0|1'],
        ['1|0', '1|0']], dtype='<U3'),
 array([2, 2, 2, 1]))
```

It is worth noting that the original algorithm of Small[37] for mapping time series into ordinal networks uses a different approach for creating the symbolic sequence. Instead of defining overlapping partitions (Eq. 1), Small[37] evaluates the ordinal patterns in non-overlapping partitions of size d_x (the embedding delay is also not present in his original formulation). Furthermore, edges are undi-

rected and unweighted in this initial formulation. This implementation is not as popular as the one directly following the Bandt-Pompe symbolization method[38,81–83], but is also available in `ordpy` through the `overlapping` parameter in the `ordinal_network` function, as shown in:

```
>>> from ordpy import ordinal_network
>>> ordinal_network([4,7,9,10,6,11,8,3,7],
... dx=2, normalized=False,
... overlapping=False)
(array(['0|1', '1|0'], dtype='<U3'),
array([['0|1', '0|1'], ['0|1', '1|0']],
dtype='<U3'), array([2, 1]))
```

Ordinal networks have also been recently generalized by Pessa and Ribeiro[41] to account for two-dimensional data sets such as images. In this case, we apply the two-dimensional version of Bandt and Pompe's symbolization approach[35] (see Eqs. 5, 6, and 7) to a data array $\{y_t^u\}_{t=1,\dots,N_x}^{u=1,\dots,N_y}$ for given embedding dimensions (d_x and d_y) and embedding delays (τ_x and τ_y), obtaining the corresponding two-dimensional ordinal sequence $\{\pi_p^q\}_{p=1,\dots,n_x}^{q=1,\dots,n_y}$. Similarly to the one-dimensional case, each permutation symbol Π_i ($i = 1, \dots, n_\pi$, with $n_\pi = (d_x d_y)!$) is associated with a node in the ordinal network, and directed edges connect permutation symbols that are vertically ($\pi_p^q \to \pi_p^{q+1}$ for $q = 1, \dots, n_y - 1$) or horizontally ($\pi_p^q \to \pi_{p+1}^q$ for $p = 1, \dots, n_x - 1$) adjacents in the symbolic sequence. The directed link between a pair of permutation symbols (Π_i and Π_j) is weighted by the total number of occurrences of this particular transition in the symbolic sequence. Thus, the weighted adjacency matrix representing the ordinal network mapped from two-dimensional data is[41]

$$\rho_{i,j} = \frac{\text{total of transitions } \Pi_i \to \Pi_j \text{ in } \{\pi_p^q\}_{p=1,\dots,n_x}^{q=1,\dots,n_y}}{2n_x n_y - n_x - n_y}, \quad (22)$$

where $i, j = 1, \dots, n_\pi$ (with $n_\pi = (d_x d_y)!$) and the denominator represents the total number of horizontal and vertical transitions. The `ordinal_network` function also handles two-dimensional data as in:

```
>>> from ordpy import ordinal_network
>>> ordinal_network([[1,2,1],[8,3,4],[6,7,5]],
... dx=2, dy=2, normalized=False)
(array(['0|1|3|2', '1|0|2|3', '1|2|3|0'],
dtype='<U7'),
 array([['0|1|3|2', '1|0|2|3'],
        ['0|1|3|2', '1|2|3|0'],
        ['1|0|2|3', '0|1|3|2'],
        ['1|2|3|0', '0|1|3|2']], dtype='<U7'),
 array([1, 1, 1, 1]))
```

Pessa and Ribeiro[41] have also proposed to create ordinal networks by considering only horizontal (horizontal ordinal networks) or only vertical (vertical ordinal networks) transitions among the permutations symbols.

They have shown that comparing properties of these two networks is useful for exploring visual symmetries in images. In `ordpy`, this possibility is available through the `connections` parameter in the `ordinal_network` function as in:

```
>>> from ordpy import ordinal_network
>>> ordinal_network([[1,2,1],[8,3,4],[6,7,5]],
... dx=2, dy=2, normalized=False,
... connections='horizontal')
(array(['0|1|3|2', '1|0|2|3', '1|2|3|0'],
dtype='<U7'),
array([['0|1|3|2', '1|0|2|3'],
        ['1|2|3|0', '0|1|3|2']], dtype='<U7'),
array([1, 1]))
```

An intriguing feature of ordinal networks is the existence of intrinsic connectivity constraints[40,41] inherited from Bandt and Pompe's symbolization method. These constraints are directly related to the fact that adjacent partitions share elements, such that ordering relations in one partition are partially carried out to neighboring partitions. For one-dimensional data, these restrictions imply that all nodes in an ordinal network have in-degree and out-degree limited to numbers between 0 and d_x; consequently, the maximum number of edges is $d_x \times (d_x!)$[40]. Ordinal networks mapped from one-dimensional data can only have self-loops in nodes associated with solely ascending or solely descending ordinal patterns[40].

The horizontal and vertical transitions related to networks mapped from two-dimensional data impose similar but trickier connectivity constraints[41]. In this case, the maximum number of outgoing connections emerging from horizontal and vertical transitions are $C(d_x d_y, d_y) \times d_y!$ and $C(d_x d_y, d_x) \times d_x!$, respectively[41]. However, the sets of horizontal and vertical transitions are not disjoint, and their union defines all possible outgoing edges. Finding a general expression for the latter set operation is cumbersome because it depends on the ordinal pattern associated with the node under analysis. Thus, while limited, the maximum number of edges varies among the ordinal patterns and needs to be numerically obtained[41]. Furthermore, differently from the one-dimensional case, ordinal networks mapped from two-dimensional data can display self-loops in several nodes[41].

A direct consequence of these intrinsic connectivity constraints is that ordinal networks mapped from completely random arrays (in one or two dimensions) are not random graphs[40,41]. Even more counter-intuitive is the existence of different edge weights in random ordinal networks, albeit all permutations are equiprobable in random arrays[40,41]. This non-trivial property results from the fact that, among all possible amplitude relations involved in an ordinal transition between a fixed permutation and all its possible neighboring permutations, some permutations appear more than once. For one-dimensional data, random ordinal networks only have two different edge weights: $1/(d_x+1)!$ and $2/(d_x+1)!$ (the

denominator represents the sum of weights)[40]. A rule of thumb for determining the edges with double weight is to pick all transitions in which the index number equal to "d_x-1" in the next permutation fits the position of the index number "0" in the first permutation[40]. For instance, the edge weight between permutations $(3,2,1,0)$ and $(2,1,0,3)$ has double weight. Ordinal networks mapped from two-dimensional random data have more than two different edge weights, and there is no simple rule (at least up to now) for obtaining these weights[41]. However, these values can be numerically calculated by explicitly considering each possible ordinal pattern[41].

In `ordpy`, the `random_ordinal_network` function generates the exact form of ordinal networks expected from the mapping of one- and two-dimensional random data with arbitrary embedding dimensions (d_x and d_y). The following code illustrates the usage of `random_ordinal_network`:

```
>>> from ordpy import random_ordinal_network
>>> random_ordinal_network(dx=2)
(array(['0|1', '1|0'], dtype='<U3'),
 array([['0|1', '0|1'],
        ['0|1', '1|0'],
        ['1|0', '0|1'],
        ['1|0', '1|0']], dtype='<U3'),
 array([0.16666667, 0.33333333,
        0.33333333, 0.16666667]))
```

The three returned arrays represent nodes, edges, and edge weights of the random ordinal network, respectively. It is worth noticing that these connectivity constraints disappear when considering non-overlapping data partitions as in the initial proposal of Small[37]. In this case, ordinal networks mapped from large enough random data sets are represented by complete graphs with self-loops and all-equal edge weights. The `random_ordinal_network` function returns these graphs by changing its `overlapping` argument as in:

```
>>> from ordpy import random_ordinal_network
>>> random_ordinal_network(dx=2,
... overlapping=False)
(array(['0|1', '1|0'], dtype='<U3'),
 array([['0|1', '0|1'],
        ['0|1', '1|0'],
        ['1|0', '0|1'],
        ['1|0', '1|0']], dtype='<U3'),
 array([0.25, 0.25, 0.25, 0.25]))
```

Similarly, embedding delays larger than one modify how elements are shared among partitions and impose connectivity constraints to high-order transitions. The `random_ordinal_network` function is thus restricted to the case $\tau_x = \tau_y = 1$ when considering overlapping partitions.

The primary purpose of mapping time series or images into ordinal networks is to use network measures to characterize data sets. In addition to the many network statistics derived from network science[85], the in-

herent probabilistic nature of nodes and edges in ordinal networks has motivated two entropy-related measures[39,40,81]. The first one is a local measure defined at the node level known as the local node entropy[39–41,81]

$$s_i = -\sum_{j\in\mathcal{O}_i} \rho'_{i,j} \log \rho'_{i,j}, \qquad (23)$$

where the index i refers to a node related to a given permutation Π_i, $\rho'_{i,j} = \rho_{i,j}/\sum_{k\in\mathcal{O}_i}\rho_{i,k}$ represents the renormalized probability of transitioning from node i to node j (permutations Π_i and Π_j), and $\mathcal{O}_i$ is the outgoing neighborhood of node i (set of all edges leaving node i). This quantity measures the determinism of ordinal transitions at the node level such that s_i is maximum when all edges leaving i have the same weight, while $s_i = 0$ if there is only one edge leaving node i. Using the local node entropy, we can further define the global node entropy[39–41,81]

$$S_{\mathrm{GN}} = \sum_{i=1}^{n_\pi} \rho_i s_i \,, \qquad (24)$$

where ρ_i is the probability of finding the permutation Π_i (Eqs. 2 and 8). Thus, the value S_{GN} represents a weighted average of the local determinism over all nodes of an ordinal network (see also Unakafov and Keller[18] for the definition of conditional entropy of ordinal patterns). In image classification tasks[41], global node entropy has proven to outperform different image quantifiers derived from gray-level co-occurrence matrices (GLCMs)[86,87], a traditional technique for texture analysis.

Contrarily to permutation entropy[4] and because of the intrinsic connectivity constraints of ordinal networks, the global node entropy is not maximized by random data[40,41]. For one-dimensional data, the global node entropy calculated from a random ordinal network is[40]

$$S_{\mathrm{GN}}^{\mathrm{random}} = \log(d_x+1) - (\log 4)/(d_x+1)\,. \qquad (25)$$

While there is no equivalent expression for two-dimensional data, it is possible to numerically calculate $S_{\mathrm{GN}}^{\mathrm{random}}$ using random ordinal networks numerically generated[41]. In both cases, the global node entropy can be normalized by the value of $S_{\mathrm{GN}}^{\mathrm{random}}$, that is, $H_{\mathrm{GN}} = S_{\mathrm{GN}}/S_{\mathrm{GN}}^{\mathrm{random}}$.

In `ordpy`, the `global_node_entropy` function evaluates S_{GN} directly from data arrays or using an ordinal network as returned by `ordinal_network`. The following code shows simple usages of `global_node_entropy`:

```
>>> from ordpy import global_node_entropy
>>> global_node_entropy(
... [1,2,3,4,5,6,7,8,9], dx=2)
0.0
>>> global_node_entropy(
... ordinal_network([1,2,3,4,5,6,7,8,9],
... dx=2))
0.0
>>> global_node_entropy(
... np.random.uniform(size=100000), dx=3)
```
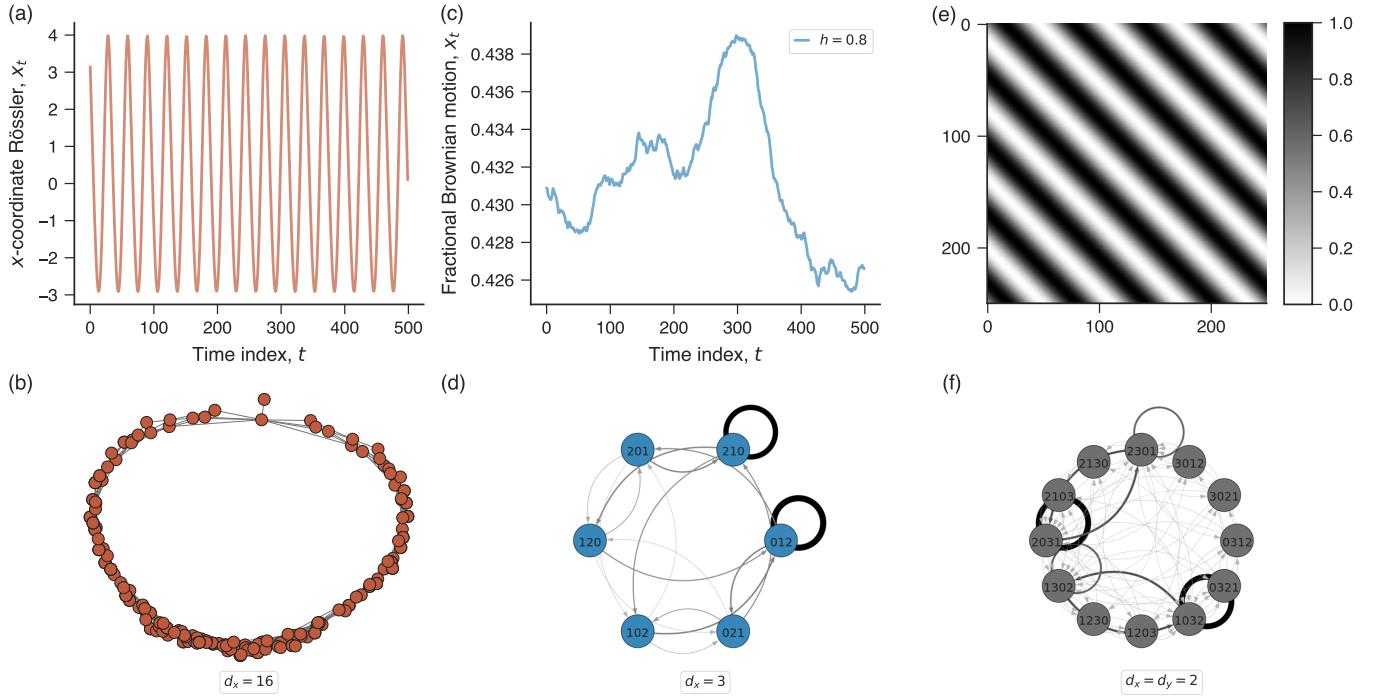
FIG. 7. Ordinal networks mapped from one- and two-dimensional data. (a) Time series obtained from the x-coordinate of the Rössler system (with parameters $a = 0.3$, $b = 2$ and $c = 4$). Here we show only the latest 500 of all 10^5 observations. This time series exhibits a periodic behavior after a short initial transient. (b) Visualization of the ordinal network mapped from the x-coordinate of the Rössler system with embedding parameters $d_x = 16$ and $\tau_x = 1$. This ordinal network uses Small's original algorithm[37] with non-overlapping data partitions and undirected and unweighted edges. (c) Time series obtained from a realization of the fractional Brownian motion with $h = 0.8$ (only the latest 500 of all 2^{16} observations are shown). (d) Ordinal network representation of the fractional Brownian motion time series with $d_x = 3$ and $\tau_x = 1$. Here we have used overlapping data partitions and made edge thickness proportional to edge weight. (e) Example of a periodic ornament with size 250×250. (f) Ordinal network representation of the previous image with embedding parameters $d_x = d_y = 2$ and $\tau_x = \tau_y = 1$. In this visualization, edge thickness is made proportional to edge weight. Data and code necessary to reproduce these results are available in a Jupyter notebook at `ordpy`'s webpage.

```
1.4988332319747597
>>> global_node_entropy(
... random_ordinal_network(dx=3))
1.5
```

VII. APPLICATIONS OF ORDINAL NETWORKS WITH `ORDPY`

To better illustrate the use of `ordpy` in the context of ordinal networks, we review and replicate some literature results. Before starting, we remark that `ordpy` does not have functions for network analysis or graph visualization. The `ordinal_network` function generates output data (nodes, edges and weight lists) that can feed graph libraries such as `graph_tool`[88], `networkx`[89], and `igraph`[90]. Here, we have used `networkx` and `igraph`.

We start by partially reproducing Small's[37] pioneering work in which "ordinal partition networks" first appeared (see Fig. 3 in that work). By following Small[37], we numerically solve the differential equations of the Rössler system (with parameters $a = 0.3$, $b = 2$ and $c = 4$, see

Appendix B for definitions) and sample the x-coordinate to obtain a time series with 10^5 observations. Figure 7a illustrates the periodic behavior of this time series. We then create the ordinal network from this data set with embedding parameters $d_x = 16$ and $\tau_x = 1$. It is worth remembering that Small's original algorithm uses non-overlapping partitions and the edges of the resulting ordinal network are undirected and unweighted. The parameter `overlapping` in `ordinal_network` should be equal to `False` to properly use Small's original algorithm. Figure 7b shows a visualization of this ordinal network, where the circular structure alludes to the periodicity of the original time series.

In another simple example with ordinal networks, we partially replicate Pessa and Ribeiro's[40] results on fractional Brownian motion (see Fig. 6 in their work). To do so, we generate a time series from this stochastic process with Hurst exponent $h = 0.8$ (see Appendix C for definitions) and 2^{16} observations, as illustrated in Fig. 7c. Next, we map this time series into an ordinal network with embedding parameters $d_x = 3$ and $\tau_x = 1$ (this time using overlapping partitions as in the usual Bandt-Pompe
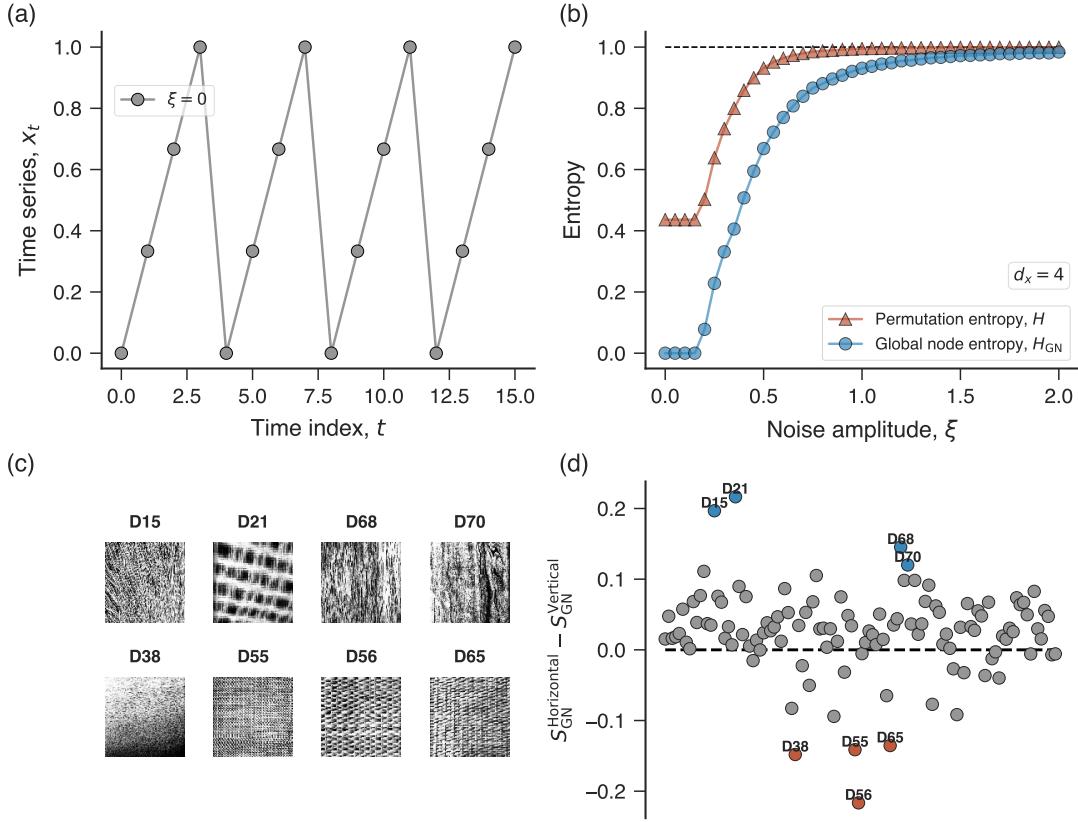
FIG. 8. Global node entropy of one- and two-dimensional data. (a) The initial data points of a sawtooth-like time series defined as $x_t = \{0, 1/3, 1/6, 1, \dots\}$. (b) Normalized permutation entropy (H) and normalized global node entropy (H_{GN}) as a function of the amplitude (ξ) of the uniform white noise added to the periodic sawtooth-like signals. The different curves represent average values of H and H_{GN} over ten realizations for $\xi = \{0, 0.05, 0.1, \dots, 2\}$. (c) Eight examples (out of 112) of the normalized Brodatz textures. These are grayscale images (256 gray levels) with size 640×640[91]. (d) Differences between the global node entropy evaluated from the horizontal and vertical ordinal networks ($S_{\mathrm{GN}}^{\mathrm{Horizontal}} - S_{\mathrm{GN}}^{\mathrm{Vertical}}$) mapped from each Brodatz texture. We highlight eight textures (the same as shown in panel c) with the largest differences. Data and code necessary to reproduce these results are available in a Jupyter notebook at `ordpy`'s webpage.

approach). Figure 7d shows a visualization of the resulting ordinal network, where the persistent behavior imposed by the Hurst exponent $h = 0.8$ is captured by the quite intense autoloops associated with the ordinal patterns $(0, 1, 2)$ and $(2, 1, 0)$ (that is, the upward and downward trends of this time series). Pessa and Ribeiro[40] have also shown that local properties of ordinal networks (for instance, average weighted shortest path) are quite effective for estimating the Hurst exponent of time series, having performance superior to widely used approaches such as detrended fluctuation analysis (DFA)[92].

We also consider ordinal networks mapped from two-dimensional data. We map a periodic ornament previously explored in Ref. 41 (see Fig. 2 in that reference). Figure 7e shows the ornament of size 250×250 (see Appendix C for more details), while Fig. 7f presents a visualization of the corresponding ordinal network with embedding parameters $d_x = d_y = 2$ and $\tau_x = \tau_y = 1$. We have made edge thickness proportional to edge weight (Eq. 22) to highlight that a few edges concentrate most of the transition probability of the network. Furthermore, we

observe that this network has 12 nodes and 72 edges, that is, only a small fraction of all possible nodes (24) and edges (416) of a ordinal networks with $d_x = d_y = 2$ and $\tau_x = \tau_y = 1$.

In addition to the previous more qualitative examples, we have also replicated some results related to the global node entropy of ordinal networks. For time series, we follow Pessa and Ribeiro[40] (see Fig. 5 in their work) and generate a periodic sawtooth-like signal (Fig. 8a) with 10^5 observations and add to it uniform white noise in the interval $[-\xi, \xi]$, where ξ represents the noise amplitude. We generate these noisy sawtooth-like time series for each $\xi \in \{0, 0.05, 0.1, \dots, 2\}$ and determine the average values of the normalized permutation entropy (H) and the normalized global node entropy (H_{GN}) over ten time series replicas with $d_x = 4$ and $\tau_x = 1$.

Figure 8b shows the average values of H and H_{GN} as a function of the noise amplitude ξ. We note that both measures approach one with the increase of the noise amplitude. However, permutation entropy saturates for $\xi \approx 1$, while global node entropy requires significantly

higher values of ξ. This result indicates that global node entropy is more robust to noise addition and has a higher discrimination power than permutation entropy[40].

To demonstrate the use of `global_node_entropy` with two-dimensional data, we calculate the global node entropy for a set of 112 8-bit images of natural textures known as the normalized Brodatz textures[91,93]. Figure 8c shows examples of these images. By following Pessa and Ribeiro[41] (see Fig. 5 in their work), we calculate the global node entropy from the horizontal ($S_{\mathrm{GN}}^{\mathrm{Horizontal}}$) and vertical ($S_{\mathrm{GN}}^{\mathrm{Vertical}}$) ordinal networks mapped from the Brodatz textures with $d_x = d_y = 2$ and $\tau_x = \tau_y = 1$.

Figure 8d depicts the difference between these two entropy values (that is, $S_{\mathrm{GN}}^{\mathrm{Horizontal}} - S_{\mathrm{GN}}^{\mathrm{Vertical}}$) for each Brodatz texture. We have also highlighted eight textures with extreme values for this difference. Most of these images are characterized by stripes or line segments predominantly oriented in the vertical or horizontal directions which, in turn, suggests that properties of vertical and horizontal ordinal networks can detect simple image symmetries.

In a final application with ordinal networks, we explore the concept of missing links or missing transitions among ordinal patterns[40]. Similarly to the missing ordinal patterns described by Amigó et al.[65,67], ordinal networks can display true and false forbidden transitions among ordinal patterns. In this case, true missing links are related to the intrinsic dynamics of the process under analysis, while false missing links are associated with the finite size of empirical data sets. Because we know the exact form of random ordinal networks[40,41] (here these networks represent all possible connections) we can readily find all missing links of an empirical ordinal network. In `ordpy`, the `missing_links` function evaluates all missing ordinal transitions directly from a data set or the returned arrays of `ordinal_network` as in:

```
>>> from ordpy import missing_links
>>> missing_links([4,7,9,10,6,11,3], dx=2,
... return_fraction=False)
(array([['1|0', '1|0']], dtype='<U3'), 1)
>>> missing_links(ordinal_network(
... [4,7,9,10,6,11,3],  dx=2),
... dx=2, return_fraction=True)
(array([['1|0', '1|0']], dtype='<U3'), 0.25)
```

To demonstrate the use of `missing_links` in a more engaging example, we replicate the results of Pessa and Ribeiro[40] about missing links in ordinal networks mapped from Gaussian white noise time series (Fig. 4 in their work). We generate these time series with length N_x varying logarithmically between 10 and 10^5, and for each one, we estimate the average fraction of missing links over ten replicas for embedding dimensions $d_x \in \{3, 4, 5, 6\}$ and $\tau_x = 1$. Figure 9a shows these fractions of missing links as a function of the time series length. We observe that this quantity approaches zero as N_x becomes sufficiently large. Furthermore, the smaller the embedding dimen-

sion, the faster the missing links vanish. This pattern is a fingerprint of false missing links. We have also carried out the same analysis with time series generated from logistic map iterations at fully developed chaos. Figure 9b shows the corresponding results. Unlike white noise, the logistic map produces ordinal networks with missing links that persist even in considerably long time series. This behavior is typical of true missing links.

VIII. CONCLUSIONS

We have introduced `ordpy` – an open-source Python module for data analysis that implements several ordinal methods associated with the Bandt-Pompe framework. Specifically, `ordpy` has functions implementing the following methods: permutation entropy, complexity-entropy plane, missing ordinal patterns, Tsallis and Rényi permutation entropies, complexity-entropy curves, ordinal networks, and missing ordinal transitions. All `ordpy`'s functions automatically deal with one-dimensional (time series) and two-dimensional (images) data. Furthermore, most of these functions are also ready for multiscale analysis via the embedding delay parameters. Along with the description of `ordpy` functionalities, we have also presented a literature review of several of the principal methods related to Bandt and Pompe's framework. This review further includes a reproduction of several literature results with `ordpy`'s functions. Beyond the summarized description of `ordpy`'s functions presented here, we notice that a complete documentation is available at `arthurpessa.github.io/ordpy`. All data and code used in this work are also freely available at `ordpy`'s website.

We believe `ordpy` will help to popularize ordinal methods even further, particularly in research fields with more limited tradition in scientific computing. In addition to a myriad of possible empirical applications, we also believe `ordpy` can further promote the development of new methods related to Bandt and Pompe's framework. We remark that some techniques available in `ordpy` have received little attention or have not even been formally proposed. These possible developments already implemented in `ordpy` include the use of complexity-entropy curves for two-dimensional data, multiscale complexity-entropy curves, ordinal networks with different embedding delays (particularly for two-dimensional data), analysis of missing patterns in two-dimensional data, and missing ordinal transitions. We also plan to implement more techniques based on the Bandt and Pompe's framework and include them in future versions of `ordpy`.

Finally, we hope our module helps making research methods more accessible and reproducible[94,95] as well as other open-source software efforts such as the `tisean`[96] (nonlinear time series analysis), `pyunicorn`[97] (time series networks and recurrence analysis), and `powerlaw`[98] (analysis of heavy-tailed distributions) packages.
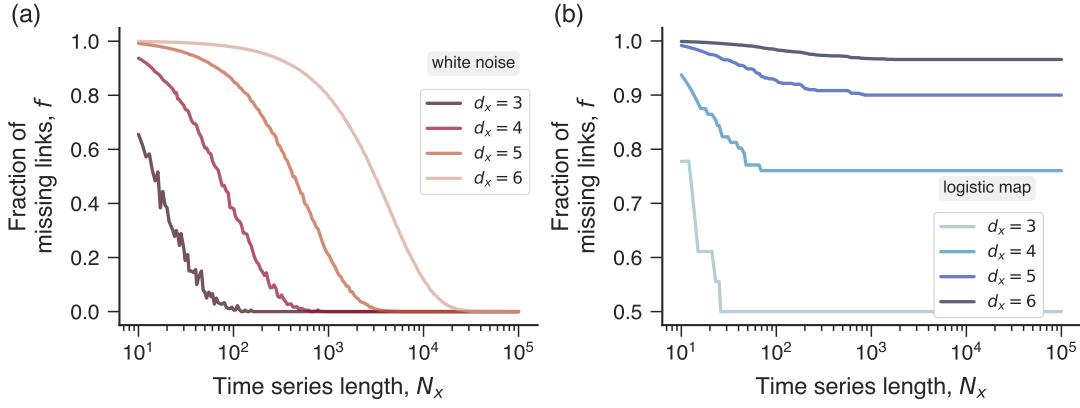
FIG. 9. True and false missing links in ordinal networks. (a) Dependence of the fraction of missing links (f) estimated from Gaussian white noise time series as a function of the time series length (N_x). (b) Dependence of the fraction of missing links (f) estimated from fully chaotic logistic time series ($r = 4$) as a function of the time series length (N_x). In both panels, the different curves represent average values over ten realizations (for each series length) and embedding dimension $d_x \in \{3, 4, 5, 6\}$ with $\tau_x = 1$. We also use 194 values for N_x logarithmically spaced in the interval $[10, 10^5]$ in both panels. Data and code necessary to reproduce these results are available in a Jupyter notebook at ordpy's webpage.

DATA AVAILABILITY

All data and code necessary to reproduce the results and figures of this work are available at http://github.com/arthurpessa/ordpy, Ref. 99.

Appendix A: Selection of embedding parameters

As we have commented in the main text, the embedding parameters (d_x and τ_x) are important for several applications related to the Bandt-Pompe framework, and wrong choices can lead to misleading conclusions. At the same time, there is no unique fail-safe procedure for selecting optimal values for these parameters, and this choice often depends on the time-series nature and the research question under analysis. In the context of permutation entropy, Myers *et al.*[53] suggest three main strategies: *i)* follow experts' suggestion; *ii)* trial and error; and *iii)* the use of nonlinear time series methods related to phase space reconstruction.

The first strategy consists of following good practices previously established in the literature, and good starting points are review articles on permutation entropy and related methods such as Refs. 10–13. The work of Riedl *et al.* is particularly interesting for this strategy as the authors compile different choices of embedding parameters according to characteristics of time series and research field. Among other propositions, these authors suggest using $\tau_x = 1$ and the largest embedding dimension yielding a proper evaluation of the ordinal distribution when dealing with data more easily described by discrete models[11].

The second strategy refers to the computational origin of the Bandt-Pompe framework, and much in line with statistical learning methods[100,101], optimal parameter selection is often achieved by experimentation (trial and error), heuristics, and validation using null models. We believe this strategy is fundamental in applications involving classification and regression tasks, where the optimal embedding parameters can be found by optimizing loss functions in cross-validation and train/test split strategies[34]. For instance, Kulp *et al.*[102] have suggested using ensemble of random series with the same length of the series under analysis and selecting the maximum embedding dimension for which the number of missing patterns is zero.

The third strategy for selecting the embedding parameters refers to using methods derived or related to nonlinear time series analysis[1,2,103]. Common techniques such as looking for the fist zero of the autocorrelation function or the first minimum of the mutual information might be especially interesting when choosing τ_x[1,103]. It is worth remembering that the concept of embedding parameters in the Bandt-Pompe approach is intimately related to the idea of embedding and phase-space reconstruction in the context of dynamical systems[104–107]. Indeed, investigations based on ordinal methods in the context of chaotic dynamics are an instrumental part for the development of the Bandt-Pompe framework[4,14,37]. In this context, a simple and interesting conceptualization on how the embedding dimension relates to the underlying phase space is presented by Groth[108].
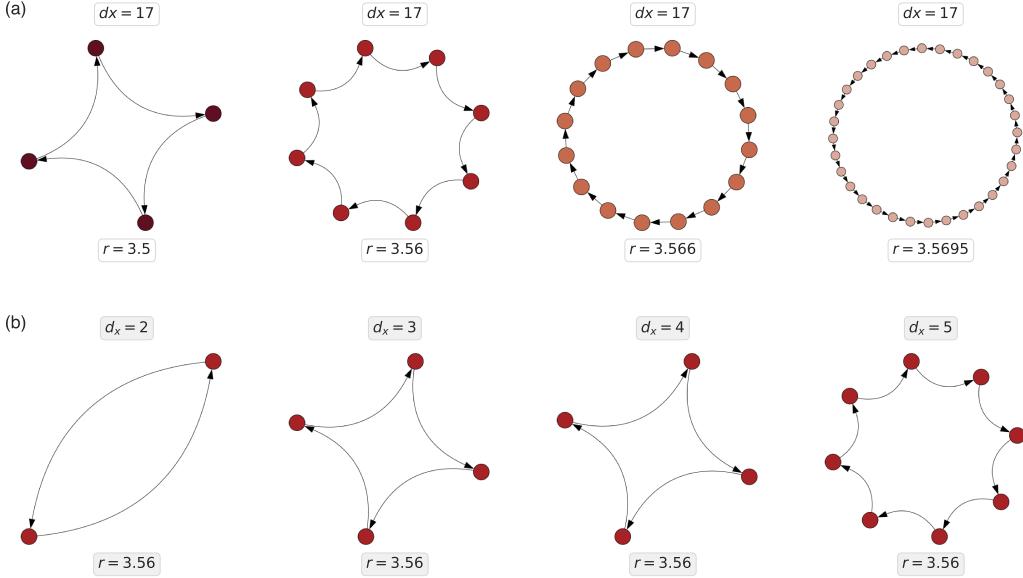
FIG. 10. Ordinal networks mapped from periodic logistic series. (a) Ordinal networks mapped from periodic logistic series ($N_x = 100$) with parameters $r = 3.5$ (period 4), $r = 3.56$ (period 8), $r = 3.566$ (period 16), and $r = 3.5695$ (period 32). All four networks are obtained with embedding parameters $d_x = 17$ and $\tau_x = 1$. (b) Ordinal networks mapped from a logistic series of period 8 ($r = 3.56$) with embedding dimensions $d_x \in \{2, 3, 4, 5\}$ and $\tau_x = 1$. We notice that d_x must be larger than 4 so that the number of nodes is equal to the time series period. We further remark that this network structure is not modified when considering values d_x larger than 4 (as shown by the second network of panel a). Data and code necessary to reproduce these results are available in a Jupyter notebook at `ordpy`'s webpage.

In addition to the previous three main strategies, there are also attempts devoted to developing automatic procedures for selecting embedding parameters in the context of permutation entropy.[11,53,109] Among these, we highlight the interesting comparison between expert recommendations and automatic approaches presented by Myers *et al.*[53]

Considering the more recent developments related to mapping time series into ordinal networks, several works on this topic have devoted efforts to the optimal selection of embedding parameters[37,38,83,110]. In this context, topological properties or network metrics have become major criteria for properly selecting embedding parameters capable of capturing dynamical features of time series. To illustrate this approach, we have partially reproduced the results of Sakellariou *et al.*[83] (see Fig. 8 in their work) about ordinal networks mapped from periodic logistic series with period 2^k for $k \in (2, 3, 4, 5)$. Figure 10a shows a representation of these networks mapped with $d_x = 17$ and $\tau_x = 1$. We observe that this value of d_x is large enough to map the periodic behavior of these time series into a regular ring-like network structure with the number of nodes precisely equal to the time series period. As discussed by Sakellariou *et al.*[83], the embedding dimension needs to be larger than 2^{k-1} so that the network topology explicitly represents the period 2^k of the time series. Figure 10b illustrates what happens with ordinal networks mapped from a period 8 time series ($k = 3$) for different values of d_x, confirming the network topol-

ogy only explicitly accounts for period 8 behavior for $d_x > 4$. Similar problems involving non-optimal choices for d_x emerge when using ordinal networks to estimate dynamical quantities such as the topological entropy[111].

Appendix B: Definitions of dynamical systems

In this appendix, we present a brief definition of the dynamical systems used in this manuscript.

1. The logistic map is defined by the following difference equation[112]:

$$x_{t+1} = rx_t(1 - x_t), \tag{B1}$$

where r is a parameter. We have used $r = 4$ in most applications of this manuscript unless specified otherwise.

2. The transient logistic map is defined as[51,113]

$$x_{t+1} = r(t)x_t(1 - x_t), \tag{B2}$$

where the parameter $r(t)$ changes at each iteration. The results of Figs. 3e and 3f were obtained with $r(t = 0) = 3.5$ and by incrementing this parameter in steps of size 10^{-4} up to $r(t) = 4$.

3. The skew tent map is defined as[114]

$$\begin{cases} x/\omega & \text{for } x \in [0, \omega] \\ (1-x)/(1-\omega) & \text{for } x \in [\omega, 1] \end{cases}, \tag{B3}$$

where ω is a parameter. In the complexity-entropy plane application shown in Fig. 4a, we have used $\omega = 0.1847$.

4. The Hénon map is defined as[115]

$$\begin{cases} x_{t+1} = 1 - ax_t^2 + y_t \\ y_{t+1} = bx_t \end{cases}, \qquad \text{(B4)}$$

where a and $|b| < 1$ are parameters. This map can be thought of as a two-dimensional extension of the logistic map[115]. We have used $a = 1.4$ and $b = 0.3$ for the results related to the complexity-entropy plane.

5. The Schuster map is defined as[115]

$$x_{t+1} = (x_t + x_t^z) \bmod 1, \qquad \text{(B5)}$$

where z is a parameter, and the modulo operation returns the fractional (decimal) part of a number. We have used $z \in \{2, 2.5, 3\}$, as shown in Fig. 4a.

6. The Rössler system is a continuous time dynamical system defined as[116,117]

$$\begin{aligned} \frac{dx}{dt} &= -y - z \\ \frac{dy}{dt} &= x + ay \qquad , \\ \frac{dz}{dt} &= b + z(x - c) \end{aligned} \qquad \text{(B6)}$$

where a, b, and c are parameters. We have numerically solved this differential equation system using the `scipy` Python module[118] with parameters $a = 0.3$, $b = 2$ and $c = 4$.

Appendix C: Definitions of stochastic processes

In this appendix, we briefly describe the stochastic processes used in the manuscript.

1. An Ising surface[119,120] is a square lattice in which the height at each lattice site represents the accumulated sum of spin variables of particles in a Monte Carlo simulation[68]. If we assume $\sigma_i \in \{-1, 1\}$ represents the spin variable at site i, we can write the Hamiltonian of this system as

$$\mathcal{H} = -\sum_{\langle i,j \rangle} \sigma_i \sigma_j, \qquad \text{(C1)}$$

where the summation is over all pairs of first neighbors in a square lattice. The height S_i at site i of the corresponding Ising surface is then defined as

$$S_i = \sum_t \sigma_i(t), \qquad \text{(C2)}$$

where $\sigma_i(t)$ is the spin value in step t of the Monte Carlo simulation. For each surface, we define the reduced temperature T_r as the ratio between the temperature T and the critical temperature T_c of the Ising system ($T_c = 2/\ln(1 + \sqrt{2})$). Finally, we have used periodic boundary conditions in our numerical experiments.

2. A fractional Brownian motion is a continuous, self-similar, and non-stationary stochastic process introduced by Mandelbrot and Van Ness[121]. The Hurst exponent $h \in (0, 1)$ controls the roughness observed in samples of this process, such that the smaller the values of h, the rougher the time series. The case $h = 1/2$ corresponds to ordinary Brownian motion (integrated Gaussian white noise). To generate samples (time series) of this stochastic process, we have used the Hosking method[122].

3. A fractional Gaussian noise is a stationary stochastic process that represents the increments of fractional Brownian motion. For this Gaussian process, the Hurst parameter $h \in (0, 1)$ controls the range of auto-correlation of the time series. For $h > 1/2$, the process presents long-range persistent memory. For $h < 1/2$, samples present anti-persistent behavior. We have Gaussian white noise if $h = 1/2$. To generate samples of a fractional Gaussian noise, we have also used the Hosking method[122,123]. More detailed information about simulations of fractional Gaussian noise and fractional Brownian motion can be found in Ref. 123. The C source code used in this work is publicly available in Ref. 124.

4. A $1/f$ noise or a Flicker noise[125,126] is a class of stochastic processes presenting a power-law power spectral density[125–127], that is, $\mathcal{P} \sim 1/f^{-k}$. The case $k = 0$ corresponds to white noise, while $k = 2$ corresponds to brown noise (random walk or integrated white noise). We have generated Gaussian distributed $1/f^{-k}$ noise for $k \in \{0, 0.25, 0.50, \ldots, 3.0\}$ with the algorithm proposed by Timmer and König[127] as implemented in Ref.[128].

5. The periodic ornament used in this work can be generated by first defining two square arrays

$$X_{i,j} = \frac{2\pi(j-1)}{(n-1)} \quad \text{and} \quad Y_{i,j} = \frac{2\pi(i-1)}{(n-1)}, \qquad \text{(C3)}$$

and next by calculating

$$Z_{i,j} = \sin\left(\frac{\omega}{2\pi} X_{i,j} \cos\theta - \frac{\omega}{2\pi} Y_{i,j} \sin\theta\right), \qquad \text{(C4)}$$

where $i, j = 1, \ldots, n$, with n being the ornament size, θ defining the stripes angle, and $\omega > 0$ the stripe frequency. The ornament shown in Fig. 7e is obtained by setting $n = 250$, $\omega = 9$ and $\theta = 135$ degrees. Previous works[36,41,129] have also considered shuffled versions of this periodic ornament, where a parameter controls the fraction of elements $Z_{i,j}$ that are randomly shuffled. A function implementing this geometric ornament is available in `ordpy`'s notebook.

[1]H. Kantz and T. Schreiber, *Nonlinear Time Series Analysis* (Cambridge University Press, New York, 2004).

[2]E. Bradley and H. Kantz, "Nonlinear time-series analysis revisited," Chaos **25**, 097610 (2015).

[3]C. E. Shannon, "A mathematical theory of communication," The Bell System Technical Journal **27**, 379–423 (1948).

[4] C. Bandt and B. Pompe, "Permutation entropy: A natural complexity measure for time series," Physical Review Letters **88**, 174102 (2002).

[5] N. Nicolaou and J. Georgiou, "Detection of epileptic electroencephalogram based on permutation entropy and support vector machines," Expert Systems with Applications **39**, 202–209 (2012).

[6] L. Zunino, M. Zanin, B. M. Tabak, D. G. Pérez, and O. A. Rosso, "Forbidden patterns, permutation entropy and stock market inefficiency," Physica A **388**, 2854–2864 (2009).

[7] J. Garland, T. Jones, M. Neuder, V. Morris, J. White, and E. Bradley, "Anomaly detection in paleoclimate records using permutation entropy," Entropy **20**, 931 (2018).

[8] R. Yan, Y. Liu, and R. X. Gao, "Permutation entropy: A nonlinear statistical measure for status characterization of rotary machines," Mechanical Systems and Signal Processing **29**, 474–484 (2012).

[9] M. Matilla-García and M. Ruiz Marín, "A non-parametric independence test using permutation entropy," Journal of Econometrics **144**, 139–155 (2008).

[10] M. Zanin, L. Zunino, O. A. Rosso, and D. Papo, "Permutation entropy and its main biomedical and econophysics applications: A review," Entropy **14**, 1553–1577 (2012).

[11] M. Riedl, A. Müller, and N. Wessel, "Practical considerations of permutation entropy," The European Physical Journal Special Topics **222**, 249–262 (2013).

[12] J. M. Amigó, K. Keller, and V. A. Unakafova, "Ordinal symbolic analysis and its application to biomedical recordings," Philosophical Transactions of the Royal Society A **373**, 20140091 (2015).

[13] K. Keller, T. Mangold, I. Stolz, and J. Werner, "Permutation entropy: New ideas and challenges," Entropy **19**, 134 (2017).

[14] O. A. Rosso, H. A. Larrondo, M. T. Martin, A. Plastino, and M. A. Fuentes, "Distinguishing noise from chaos," Physical Review Letters **99**, 154102 (2007).

[15] L. Zunino, D. Pérez, A. Kowalski, M. Martín, M. Garavaglia, A. Plastino, and O. Rosso, "Fractional Brownian motion, fractional Gaussian noise, and Tsallis permutation entropy," Physica A **387**, 6057–6068 (2008).

[16] L. C. Carpi, P. M. Saco, and O. Rosso, "Missing ordinal patterns in correlated noises," Physica A **389**, 2020–2029 (2010).

[17] U. Parlitz, S. Berg, S. Luther, A. Schirdewan, J. Kurths, and N. Wessel, "Classifying cardiac biosignals using ordinal pattern statistics and symbolic dynamics," Computers in Biology and Medicine **42**, 319–327 (2012).

[18] A. M. Unakafov and K. Keller, "Conditional entropy of ordinal patterns," Physica D **269**, 94–102 (2014).

[19] Z. Liang, Y. Wang, X. Sun, D. Li, L. J. Voss, J. W. Sleigh, S. Hagihira, and X. Li, "EEG entropy measures in anesthesia," Frontiers in Computational Neuroscience **9**, 16 (2015).

[20] Y. Ruan, R. V. Donner, S. Guan, and Y. Zou, "Ordinal partition transition network based complexity measures for inferring coupling direction and delay from time series," Chaos **29**, 043111 (2019).

[21] L. Zunino, F. Olivares, and O. A. Rosso, "Permutation min-entropy: An improved quantifier for unveiling subtle temporal correlations," EPL (Europhysics Letters) **109**, 10005 (2015).

[22] C. Bandt, "A new kind of permutation entropy used to classify sleep stages from invisible EEG microstructure," Entropy **19**, 197 (2017).

[23] H. V. Ribeiro, M. Jauregui, L. Zunino, and E. K. Lenzi, "Characterizing time series via complexity-entropy curves," Physical Review E **95**, 062106 (2017).

[24] M. Jauregui, L. Zunino, E. K. Lenzi, R. S. Mendes, and H. V. Ribeiro, "Characterization of time series via Rényi complexity-entropy curves," Physica A **498**, 74–85 (2018).

[25] W. Aziz and M. Arif, "Multiscale permutation entropy of physiological time series," in 2005 Pakistan Section Multitopic Conference (IEEE, 2005) pp. 1–6.

[26] L. Zunino, M. C. Soriano, I. Fischer, O. A. Rosso, and C. R. Mirasso, "Permutation-information-theory approach to unveil delay dynamics from time-series analysis," Physical Review E **82**, 046212 (2010).

[27] F. C. Morabito, D. Labate, F. L. Foresta, A. Bramanti, G. Morabito, and I. Palamara, "Multivariate multi-scale permutation entropy for complexity analysis of Alzheimer's disease EEG," Entropy **14**, 1186–1202 (2012).

[28] L. Zunino, M. C. Soriano, and O. A. Rosso, "Distinguishing chaotic and stochastic dynamics from time series by using a multiscale symbolic approach," Physical Review E **86**, 046210 (2012).

[29] B. Fadlallah, B. Chen, A. Keil, and J. Príncipe, "Weighted-permutation entropy: A complexity measure for time series incorporating amplitude information," Physical Review E **87**, 022911 (2013).

[30] J. Xia, P. Shang, J. Wang, and W. Shi, "Permutation and weighted-permutation entropy analysis for the complexity of nonlinear time series," Communications in Nonlinear Science and Numerical Simulation **31**, 60–68 (2016).

[31] H. Azami and J. Escudero, "Amplitude-aware permutation entropy: Illustration in spike detection and signal segmentation," Computer Methods and Programs in Biomedicine **128**, 40–51 (2016).

[32] S. Chen, P. Shang, and Y. Wu, "Weighted multiscale Rényi permutation entropy of nonlinear time series," Physica A **496**, 548–570 (2018).

[33] C. Bian, C. Qin, Q. D. Y. Ma, and Q. Shen, "Modified permutation-entropy analysis of heartbeat dynamics," Physical Review E **85**, 021906 (2012).

[34] D. Cuesta-Frau, M. Varela-Entrecanales, A. Molina-Picó, and B. Vargas, "Patterns with equal values in permutation entropy: Do they really matter for biosignal classification?" Complexity **2018**, 1324696 (2018).

[35] H. V. Ribeiro, L. Zunino, E. K. Lenzi, P. A. Santoro, and R. S. Mendes, "Complexity-entropy causality plane as a complexity measure for two-dimensional patterns," PLoS One **7**, 1–9 (2012).

[36] L. Zunino and H. V. Ribeiro, "Discriminating image textures with the multiscale two-dimensional complexity-entropy causality plane," Chaos, Solitons & Fractals **91**, 679–688 (2016).

[37] M. Small, "Complex networks from time series: Capturing dynamics," in 2013 IEEE International Symposium on Circuits and Systems (ISCAS2013) (2013) pp. 2509–2512.

[38] M. McCullough, M. Small, T. Stemler, and H. H.-C. Iu, "Time lagged ordinal partition networks for capturing dynamics of continuous dynamical systems," Chaos **25**, 053101 (2015).

[39] M. Small, M. McCullough, and K. Sakellariou, "Ordinal network measures — quantifying determinism in data," in 2018 IEEE International Symposium on Circuits and Systems (ISCAS) (2018) pp. 1–5.

[40] A. A. B. Pessa and H. V. Ribeiro, "Characterizing stochastic time series with ordinal networks," Physical Review E **100**, 042304 (2019).

[41] A. A. B. Pessa and H. V. Ribeiro, "Mapping images into ordinal networks," Physical Review E **102**, 052312 (2020).

[42] J. B. Borges, H. S. Ramos, R. A. F. Mini, O. A. Rosso, A. C. Frery, and A. A. F. Loureiro, "Learning and distinguishing time series dynamics via ordinal patterns transition graphs," Applied Mathematics and Computation **362**, 124554 (2019).

[43] E. T. C. Chagas, A. C. Frery, O. A. Rosso, and H. S. Ramos, "Characterization of SAR images with weighted amplitude transition graphs," in 2020 IEEE Latin American GRSS ISPRS Remote Sensing Conference (LAGIRS) (2020) pp. 264–269.

[44] "The data deluge," Available: https://www.economist.com/leaders/2010/02/25/the-data-deluge (2010), Accessed: 20 Oct 2020.

[45] C. A. Mattmann, "A vision for data science," Nature **493**, 473–475 (2013).

[46] D. M. Blei and P. Smyth, "Science and data science," Proceedings of the National Academy of Sciences **114**, 8689–8692 (2017).

[47] C. R. Harris, K. J. Millman, S. J. van der Walt, R. Gommers, P. Virtanen, D. Cournapeau, E. Wieser, J. Taylor, S. Berg, N. J. Smith, R. Kern, M. Picus, S. Hoyer, M. H. van Kerkwijk, M. Brett, A. Haldane, J. F. del Río, M. Wiebe, P. Peterson, P. Gérard-Marchant, K. Sheppard, T. Reddy, W. Weckesser, H. Abbasi, C. Gohlke, and T. E. Oliphant, "Array programming with NumPy," Nature **585**, 357–362 (2020).

[48] J. M. Perkel, "Pick up Python," Nature **518**, 125–126 (2015).

[49] H. Shen, "Interactive notebooks: Sharing the code," Nature **515**, 151–152 (2014).

[50] T. Kluyver, B. Ragan-Kelley, F. Pérez, B. Granger, M. Bussonnier, J. Frederic, K. Kelley, J. Hamrick, J. Grout, S. Corlay, P. Ivanov, D. Avila, S. Abdalla, C. Willing, and Jupyter development team, "Jupyter notebooks – a publishing format for reproducible computational workflows," in *Positioning and Power in Academic Publishing: Players, Agents and Agendas*, edited by F. Loizides and B. Scmidt (IOS Press, 2016) pp. 87–90.

[51] Y. Cao, W. wen Tung, J. B. Gao, V. A. Protopopescu, and L. M. Hively, "Detecting dynamical changes in time series using the permutation entropy," Physical Review E **70**, 046217 (2004).

[52] D. Cuesta-Frau, J. P. Murillo-Escobar, D. A. Orrego, and E. Delgado-Trejos, "Embedded dimension and time series length. Practical influence on permutation entropy and its applications," Entropy **21**, 385 (2019).

[53] A. Myers and F. A. Khasawneh, "On the automatic parameter selection for permutation entropy," Chaos **30**, 033130 (2020).

[54] L. Zunino, F. Olivares, F. Scholkmann, and O. A. Rosso, "Permutation entropy based time series analysis: Equalities in the input signal can lead to false conclusions," Physics Letters A **381**, 1883–1892 (2017).

[55] J. Amigó, S. Zambrano, and M. A. Sanjuán, "Combinatorial detection of determinism in noisy time series," EPL (Europhysics Letters) **83**, 60005 (2008).

[56] O. A. Rosso and C. Masoller, "Detecting and quantifying temporal correlations in stochastic resonance via information theory measures," The European Physical Journal B **69**, 37–43 (2009).

[57] L. Zunino, M. Zanin, B. M. Tabak, D. G. Pérez, and O. A. Rosso, "Complexity-entropy causality plane: A useful approach to quantify the stock market inefficiency," Physica A **389**, 1891–1901 (2010).

[58] L. Zunino, A. Fernández Bariviera, M. B. Guercio, L. B. Martinez, and O. A. Rosso, "On the efficiency of sovereign bond markets," Physica A **391**, 4342–4349 (2012).

[59] H. V. Ribeiro, L. Zunino, R. S. Mendes, and E. K. Lenzi, "Complexity–entropy causality plane: A useful approach for distinguishing songs," Physica A **391**, 2421–2428 (2012).

[60] H. Y. D. Sigaki, R. F. de Souza, R. T. de Souza, R. S. Zola, and H. V. Ribeiro, "Estimating physical properties from liquid crystal textures via machine learning and complexity-entropy methods," Physical Review E **99**, 013311 (2019).

[61] R. López-Ruiz, H. L. Mancini, and X. Calbet, "A statistical measure of complexity," Physics Letters A **209**, 321–326 (1995).

[62] J. Lin, "Divergence measures based on the Shannon entropy," IEEE Transactions on Information Theory **37**, 145–151 (1991).

[63] P. W. Lamberti, M. T. Martin, A. Plastino, and O. A. Rosso, "Intensive entropic non-triviality measure," Physica A **334**, 119–131 (2004).

[64] M. T. Martin, A. Plastino, and O. A. Rosso, "Generalized statistical complexity measures: Geometrical and analytical properties," Physica A **369**, 439–462 (2006).

[65] J. M. Amigó, L. Kocarev, and J. Szczepanski, "Order patterns and chaos," Physics Letters A **355**, 27–31 (2006).

[66] C. Bandt and F. Shiha, "Order patterns in time series," Journal of Time Series Analysis **28**, 646–665 (2007).

[67] J. M. Amigó, S. Zambrano, and M. A. Sanjuán, "True and false forbidden patterns in deterministic and random dynamics," EPL (Europhysics Letters) **79**, 50001 (2007).

[68] D. P. Landau and K. Binder, *A Guide to Monte Carlo Simulations in Statistical Physics* (Cambridge University Press, New York, 2009).

[69] H. Y. D. Sigaki, M. Perc, and H. V. Ribeiro, "History of art paintings through the lens of entropy and complexity," Proceedings of the National Academy of Sciences **115**, E8585–E8594 (2018).

[70] "Abstract Painting: Blue," Available: https://www.wikiart.org/en/ad-reinhardt/abstract-painting-blue-1953, Accessed: 24 Nov 2020.

[71] "Abaporu," Available: https://www.wikiart.org/en/tarsila-do-amaral/abaporu-1928, Accessed: 24 Nov 2020.

[72] "Number 1 (Lavender Mist)," Available: https://www.wikiart.org/en/jackson-pollock/number-1-lavender-mist-1950-1, Accessed: 24 Nov 2020.

[73] M. Zanin, "Forbidden patterns in financial time series," Chaos **18**, 013119 (2008).

[74] K. Sakellariou, M. McCullough, T. Stemler, and M. Small, "Counting forbidden patterns in irregularly sampled time series. II. Reliability in the presence of highly irregular sampling," Chaos **26**, 123104 (2016).

[75] M. McCullough, K. Sakellariou, T. Stemler, and M. Small, "Counting forbidden patterns in irregularly sampled time series. I. The effects of under-sampling, random depletion, and timing jitter," Chaos **26**, 123103 (2016).

[76] C. W. Kulp, J. M. Chobot, B. J. Niskala, and C. J. Needhammer, "Using forbidden ordinal patterns to detect determinism in irregularly sampled time series," Chaos **26**, 023107 (2016).

[77] C. Tsallis, "Possible generalization of Boltzmann-Gibbs statistics," Journal of Statistical Physics **52**, 479–487 (1988).

[78] A. Rényi, "On measures of entropy and information," in *Proceedings of the Fourth Berkeley Symposium on Mathematical Statistics and Probability, Volume 1: Contributions to the Theory of Statistics* (University of California Press, Berkeley, 1961) pp. 547–561.

[79] C. Tsallis, *Introduction to Nonextensive Statistical Mechanics: Approaching a Complex World* (Springer, New York, 2009).

[80] T. van Erven and P. Harremos, "Rényi divergence and Kullback-Leibler divergence," IEEE Transactions on Information Theory **60**, 3797–3820 (2014).

[81] M. McCullough, M. Small, H. H. C. Iu, and T. Stemler, "Multiscale ordinal network analysis of human cardiac dynamics," Philosophical Transactions of the Royal Society A **375**, 20160292 (2017).

[82] X. Sun, M. Small, Y. Zhao, and X. Xue, "Characterizing system dynamics with a weighted and directed network constructed from time series data," Chaos **24**, 024402 (2014).

[83] K. Sakellariou, T. Stemler, and M. Small, "Markov modeling via ordinal partitions: An alternative paradigm for network-based time-series analysis," Physical Review E **100**, 062307 (2019).

[84] Y. Zou, R. V. Donner, N. Marwan, J. F. Donges, and J. Kurths, "Complex network approaches to nonlinear time series analysis," Physics Reports **787**, 1–97 (2019).

[85] M. Newman, *Networks: An Introduction* (Oxford University Press, New York, 2010).

[86] R. M. Haralick, K. Shanmugam, and I. H. Dinstein, "Textural features for image classification," IEEE Transactions on Systems, Man, and Cybernetics **3**, 610–621 (1973).

[87] R. M. Haralick, "Statistical and structural approaches to texture," Proceedings of the IEEE **67**, 786–804 (1979).

[88] T. P. Peixoto, "The graph-tool Python library," figshare (2014), 10.6084/m9.figshare.1164194.

[89] A. A. Hagberg, D. A. Schult, and P. J. Swart, "Exploring network structure, dynamics, and function using networkX," in *Proceedings of the 7th Python in Science Conference*, edited by G. Varoquaux, T. Vaught, and J. Millman (Pasadena, 2008) pp. 11–15.

[90] G. Csardi and T. Nepusz, "The igraph software package for complex network research," InterJournal **Complex Systems**, 1695 (2006).

[91] Centre for Research and Applications in Remote Sensing (CARTEL, University of Sherbrooke), "Multiband texture

[91]database," Available: https://multibandtexture.recherche.usherbrooke.ca/normalized_brodatz.html, Accessed: 18 Dez 2020.

[92]C.-K. Peng, S. V. Buldyrev, S. Havlin, M. Simons, H. E. Stanley, and A. L. Goldberger, "Mosaic organization of DNA nucleotides," Physical Review E 49, 1685–1689 (1994).

[93]A. Safia and D.-C. He, "New Brodatz-based image databases for grayscale color and multiband texture analysis," ISRN Machine Vision 2013, 14 (2013).

[94]M. Baker, "1,500 scientists lift the lid on reproducibility," Nature 533, 452–454 (2016).

[95]D. Fanelli, "Opinion: Is science really facing a reproducibility crisis, and do we need it to?" Proceedings of the National Academy of Sciences 115, 2628–2631 (2018).

[96]R. Hegger, H. Kantz, and T. Schreiber, "Practical implementation of nonlinear time series methods: The TISEAN package," Chaos 9, 413–435 (1999).

[97]J. F. Donges, J. Heitzig, B. Beronov, M. Wiedermann, J. Runge, Q. Y. Feng, L. Tupikina, V. Stolbova, R. V. Donner, N. Marwan, H. A. Dijkstra, and J. Kurths, "Unified functional network and nonlinear time series analysis for complex systems science: The pyunicorn package," Chaos 25, 113101 (2015).

[98]J. Alstott, E. Bullmore, and D. Plenz, "powerlaw: A Python package for analysis of heavy-tailed distributions," PLoS One 9, 1–11 (2014).

[99]A. A. B. Pessa and H. V. Ribeiro, "A python package for data analysis with permutation entropy and ordinal network methods (ordpy)," Available: https://github.com/arthurpessa/ordpy, Accessed: 11 Mar 2021.

[100]G. James, D. Witten, T. Hastie, and R. Tibshirani, An Introduction to Statistical Learning: with Applications in R, Springer Texts in Statistics (Springer, New York, 2014).

[101]A. Géron, Hands-On Machine Learning with Scikit-Learn and TensorFlow: Concepts, Tools, and Techniques to Build Intelligent Systems (O'Reilly Media, Sebastopol, 2017).

[102]C. W. Kulp, J. M. Chobot, H. R. Freitas, and G. D. Sprechini, "Using ordinal partition transition networks to analyze ECG data," Chaos 26, 073114 (2016).

[103]M. Small, Applied Nonlinear Time Series Analysis: Applications in Physics, Physiology and Finance, World Scientific series in nonlinear science, Series A (World Scientific, Singapore, 2005).

[104]N. H. Packard, J. P. Crutchfield, J. D. Farmer, and R. S. Shaw, "Geometry from a time series," Physical Review Letters 45, 712–716 (1980).

[105]M. B. Kennel, R. Brown, and H. D. I. Abarbanel, "Determining embedding dimension for phase-space reconstruction using a geometrical construction," Physical Review A 45, 3403–3411 (1992).

[106]L. Cao, "Practical method for determining the minimum embedding dimension of a scalar time series," Physica D 110, 43–50 (1997).

[107]A. M. Fraser and H. L. Swinney, "Independent coordinates for strange attractors from mutual information," Physical Review A 33, 1134–1140 (1986).

[108]A. Groth, "Visualization of coupling in time series by order recurrence plots," Physical Review E 72, 046220 (2005).

[109]X. Wang, S. Si, Y. Wei, and Y. Li, "The optimized multiscale permutation entropy and its application in compound fault diagnosis of rotating machinery," Entropy 21, 170 (2019).

[110]M. McCullough, K. Sakellariou, T. Stemler, and M. Small, "Regenerating time series from ordinal networks," Chaos 27, 035814 (2017).

[111]K. Sakellariou, T. Stemler, and M. Small, "Estimating topological entropy using ordinal partition networks," Physical Review E 103, 022214 (2021).

[112]R. M. May, "Simple mathematical models with very complicated dynamics," Nature 261, 459–467 (1976).

[113]L. L. Trulla, A. Giuliani, J. P. Zbilut, and C. L. Webber, "Recurrence quantification analysis of the logistic equation with transients," Physics Letters A 223, 255–260 (1996).

[114]H. Sakai and H. Tokumaru, "Autocorrelations of a certain chaos," IEEE Transactions on Acoustics, Speech, and Signal Processing 28, 588–590 (1980).

[115]H. G. Schuster and W. Just, Deterministic Chaos: An Introduction (Wiley, Weinheim, 2005).

[116]O. Rössler, "An equation for continuous chaos," Physics Letters A 57, 397–398 (1976).

[117]S. H. Strogatz, Nonlinear Dynamics and Chaos: With Applications to Physics, Biology, Chemistry, and Engineering (Perseus Books, New York, 1994).

[118]P. Virtanen, R. Gommers, T. E. Oliphant, M. Haberland, T. Reddy, D. Cournapeau, E. Burovski, P. Peterson, W. Weckesser, J. Bright, S. J. van der Walt, M. Brett, J. Wilson, K. Jarrod Millman, N. Mayorov, A. R. J. Nelson, E. Jones, R. Kern, E. Larson, C. Carey, İ. Polat, Y. Feng, E. W. Moore, J. Vand erPlas, D. Laxalde, J. Perktold, R. Cimrman, I. Henriksen, E. A. Quintero, C. R. Harris, A. M. Archibald, A. H. Ribeiro, F. Pedregosa, P. van Mulbregt, and SciPy 1.0 Contributors, "Scipy 1.0: Fundamental algorithms for scientific computing in Python," Nature Methods 17, 261–272 (2020).

[119]A. F. Brito, J. A. Redinz, and J. A. Plascak, "Dynamics of rough surfaces generated by two-dimensional lattice spin models," Physical Review E 75, 046106 (2007).

[120]A. F. Brito, J. A. Redinz, and J. A. Plascak, "Two-dimensional XY and clock models studied via the dynamics generated by rough surfaces," Physical Review E 81, 031130 (2010).

[121]B. B. Mandelbrot and J. W. V. Ness, "Fractional Brownian motions, fractional noises and applications," SIAM Review 10, 422–437 (1968).

[122]J. R. M. Hosking, "Modeling persistence in hydrological time series using fractional differencing," Water Resources Research 20, 1898–1908 (1984).

[123]T. Diecker, Simulation of fractional Brownian motion, Ph.D. thesis, University of Twente (2004).

[124]T. Diecker, "hosking.c," Available: http://www.columbia.edu/~ad3217/fbm/hosking.c, Accessed: 26 Nov 2020.

[125]R. F. Voss, "1/f (flicker) noise: A brief review," in 33rd Annual Symposium on Frequency Control (1979) pp. 40–46.

[126]N. J. Kasdin, "Discrete simulation of colored noise and stochastic processes and $1/f^\alpha$ power law noise generation," Proceedings of the IEEE 83, 802–827 (1995).

[127]J. Timmer and M. König, "On generating power law noise," Astronomy and Astrophysics 300, 707–710 (1995).

[128]F. Patzelt, "colorednoise.py," Available: https://github.com/felixpatzelt/colorednoise, Accessed: 26 Nov 2020.

[129]A. Brazhe, "Shearlet-based measures of entropy and complexity for two-dimensional patterns," Physical Review E 97, 061301 (2018).